

# The seismo-hydro-mechanical behaviour during deep geothermal reservoir stimulations: open questions tackled in a decameter-scale in-situ stimulation experiment

Amann Florian<sup>1)</sup>, Valentin ~~Gischig~~<sup>1</sup>Gischig<sup>2)</sup>, Keith ~~Evans~~<sup>1</sup>Evans<sup>2)</sup>, Joseph ~~Doetsch~~<sup>1</sup>Doetsch<sup>2)</sup>, Reza ~~Jalali~~<sup>1</sup>Jalali<sup>2)</sup>, Benoît ~~Valley~~<sup>2</sup>Valley<sup>3)</sup>, Hannes ~~Krietsch~~<sup>1</sup>Krietsch<sup>2)</sup>, Nathan ~~Dutler~~<sup>2</sup>Dutler<sup>3)</sup>, Linus ~~Villiger~~<sup>1</sup>Villiger<sup>2)</sup>, Bernard ~~Brixel~~<sup>1</sup>Brixel<sup>2)</sup>, Maria ~~Klepikova~~<sup>1</sup>Klepikova<sup>2)</sup>, Anniina ~~Kittilä~~<sup>1</sup>Kittilä<sup>2)</sup>, Claudio ~~Madonna~~<sup>1</sup>Madonna<sup>2)</sup>, Stefan ~~Wiemer~~<sup>1</sup>Wiemer<sup>2)</sup>, Martin O. ~~Saar~~<sup>1</sup>Saar<sup>2)</sup>, Simon ~~Loew~~<sup>1</sup>Loew<sup>2)</sup>, Thomas ~~Driesner~~<sup>1)</sup>Driesner<sup>2)</sup>, Hansruedi ~~Maurer~~<sup>1</sup>Maurer<sup>2)</sup>, Domenico ~~Giardini~~<sup>1</sup>Giardini<sup>2)</sup>,

<sup>1)</sup>RWTH Aachen, Chair of Engineering Geology and Hydrogeology, Lochnerstrasse 4-20, 52064 Aachen, Germany

<sup>2)</sup>ETH Zurich, Department of Earth Sciences, Sonneggstrasse 5, 8092 Zurich, Switzerland

<sup>3)</sup>University of Neuchâtel, Centre for Hydrogeology and Geothermics (CHYN), Laboratory of Geothermics and Reservoir Geomechanics, 2000 Neuchâtel, Switzerland

**Keywords:** Deep geothermal energy, EGS, induced seismicity, in-situ experiments, hydro-mechanical coupled processes in EGS,

## Abstract

In this contribution, we present a review of scientific research results that address seismo-hydro-mechanical coupled processes relevant for the development of a sustainable heat exchanger in low permeability crystalline rock and introduce the design of the In-situ Stimulation and Circulation (ISC) experiment at the Grimsel Test Site dedicated to study such processes under controlled conditions. The review shows that research on reservoir stimulation for deep geothermal energy exploitation has been largely based on laboratory observations, large-scale projects and numerical models. Observations of full-scale reservoir stimulations have yielded important results. However, the limited access to the reservoir and limitations in the control on the experimental conditions during deep reservoir stimulations is insufficient to resolve the details of the hydro-mechanical processes that would enhance process understanding in a way that aids future stimulation design. Small scale laboratory experiments provide ~~a fundamental insights~~ into various processes relevant for enhanced geothermal energy, but suffer from 1) difficulties and uncertainties in upscaling the results to the field-scale and 2) relatively homogeneous material and stress conditions that lead to an over-simplistic fracture flow and/or hydraulic fracture propagation behaviour that is not representative for a heterogeneous reservoir. Thus, there is a need for intermediate-scale hydraulic stimulation experiments with high experimental control that bridge the various scales, and for which access to the target rock mass with a comprehensive monitoring system is possible. ~~Only few intermediate scale hydro shearing and hydro fracturing experiments have recently been performed in a densely instrumented rock mass. No such measurements have been performed on faults in crystalline basement rocks.~~ The In-situ Stimulation and Circulation (ISC) experiment ~~currently performed~~ is designed to address open research questions in a naturally fractured and faulted crystalline rock mass at the Grimsel Test Site (Switzerland) ~~is designed to address open research questions, which could not be investigated in the required detail so far.~~ Two hydraulic injection phases were executed to enhance the permeability of the rock mass: ~~a hydro shearing phase and then a hydraulic fracturing phase.~~ During the injection phases the rock mass deformation across fractures and within intact rock, the pore pressure distribution and propagation and the micro-seismic response were monitored at a high spatial and temporal resolution.

## 1 Introduction

The necessity to produce carbon dioxide neutral electricity, ideally as base-load power (i.e., 24 hours a day, year-round) and the increased aversion to nuclear power generation have motivated global efforts to optimize methods for extracting deep geothermal energy for electricity production. However, currently, geothermal power production is limited to distinct geological conditions, where fluid flow rate in geothermal reservoirs carry sufficient heat (Saar, 2011) and/or pressure for economic power generation (Randolph and Saar, 2011a; Breede et al., 2013; Adams et al., 2015). It is widely agreed that the earth's crust holds substantially more geothermal resources than are presently being exploited (e.g., Tester et al., 2006). However, standard water- or brine-based geothermal power generation requires persistent high reservoir permeabilities of at least  $10^{-16}$  m<sup>2</sup> (Manning and Ingebritsen, 1999) and temperatures of ideally over about 170°C (e.g., Evans, 2014; Saar, to be published in 2017), as otherwise it is not economic. ~~When such temperatures are not present at relatively shallow depths of a couple of kilometres, unconventional geothermal methods need to be employed. One such approach targets wells have to be drilled to at least 5 to 6 km depth into crystalline hard rock to reach formation temperatures of approximately 170-200°C in regions with standard geothermal gradients of about 30°C/km, although such temperatures are often reached at shallower depth if there is a low thermal conductivity sedimentary cover, thus requiring wells to be drilled to at least 5 to 6 km depth into crystalline hard rock. The two main difficulties of implementing these so-called. Presently, rotary drilling to such depths is uneconomic on a routine basis. Moreover, at this depth permeability is often much less than  $10^{-16}$  m<sup>2</sup> (e.g., Manning and Ingebritsen, 1999; Saar and Manga, 2004, Achtziger-Zupančič et al., 2017), so that permeability has to be artificially enhanced to permit circulation of fluids to advectively extract the heat energy economically. Such systems are referred to as Enhanced or Engineered Geothermal Systems (EGS), originally termed Hot Dry Rock (HDR) systems (Brown et al., 2012), are that 1) rotary drilling to such depths is presently uneconomic on a routine basis and 2) permeabilities of hard rocks at those depths are typically too low (e.g., Manning and Ingebritsen, 1999; Saar and Manga, 2004) to enable circulation of fluids to advectively extract the heat (and pressure) energy economically. Consequently, EGSs~~ virtually always require hydraulic stimulation to enhance the permeability to such a degree that economic geothermal power generation becomes possible. However, the goal of controlling the permeability enhancement process sufficiently enhancing permeability has not yet been achieved in a sustained way, despite attempts since the 1970s (Evans, 2014). Additionally, induced seismicity, which almost invariably

accompanies hydraulic stimulation because of high fluid injection pressure, can be problematic inasmuch as it may reach felt or even damaging intensities (e.g., Giardini, 2009).

In this contribution, we focus on how a subsurface heat exchanger may be constructed between boreholes at depth within low-permeability rock to form EGS, where a fluid, typically water or brine, may then be circulated more easily than before. The artificially enhanced permeability needs to be high enough to reach flow rates that are commercially relevant for power production, depending on the subsurface working fluid. Larger permeability enhancements are required for water or brine than for CO<sub>2</sub>, as the latter can utilize lower temperatures and lower permeabilities for economic geothermal power generation, due to its higher energy conversion efficiency (Brown, 2000; Pruess, 2006, 2007; Randolph and Saar, 2011a, 2011b; Adams et al., 2014, 2015; Garapati et al., 2015; Buscheck, 2016). Moreover, fluid flow should occur within a large number of permeable fracture pathways that sweep a large surface area of the rock, thereby providing longevity to the system and avoiding early thermal breakthrough, such as occurred at the Rosemanowes Project (Parker, 1999) and the Hijiori Project (Tenma et al., 2008). The construction of such systems (i.e., an artificial reservoir with sufficient permeability for energy extraction) is one of the key research challenges for unlocking the large potential of deep geothermal energy. The creation of a subsurface heat-exchanger between the boreholes in the low permeability rock mass typically involves hydraulic stimulation, i.e., fluid injections, during which the pore pressure is raised in the rock mass leading to the enhancements of permeability of natural fractures and faults, and perhaps the creation of new fractures.

Hydraulic stimulation is inevitably accompanied by induced seismicity (e.g., Zoback and Harjes, 1997; Evans et al., 2005a; Davis et al., 2013; Bao and Eaton, 2016), because the slip triggered by the elevated pore pressure arising from injections may be sufficiently rapid to generate seismic waves. In shale gas- and EGS-related stimulations, clouds of small induced (micro-)seismic events are important monitoring tools for delineating the location, where rock mass volume is undergoing stimulation (e.g., Wohlhard et al., 2006). Unfortunately, seismic events induced by the stimulation injections may be large enough to be felt by local populations and even to cause infrastructure damage (e.g., in Basel, 2006; Giardini, 2009). In the past few years, induced seismicity has been recognized as a significant challenge to the widespread deployment of EGS technology. From a reservoir engineering perspective, EGS faces two competing but interrelated issues: 1) rock mass permeability must be significantly enhanced by several orders of magnitude within a sufficiently large volume to enable sustainable heat extraction over many years (i.e., 20 – 30 years) while 2) keeping the associated induced seismicity below a hazardous level (Evans et al. 2014). Designing reservoir stimulation

practices that optimize permeability creation and minimize induced seismicity requires a greatly improved understanding of the seismo-hydro-mechanical (SHM) response of the target rock mass volume. Seismo-hydro-mechanical processes relevant for stimulation involve 1) HM-coupled fluid flow and pressure propagation, 2) transient pressure- and permanent slip-dependent permeability changes, 3) fracture formation and interaction with pre-existing structures, 4) rock mass deformation around the stimulated volume due to fault slip, failure processes and poroelastic effects, and 5) the transition from aseismic to seismic slip.

~~A~~In 2017, a decameter-scale, in-situ, stimulation and circulation (ISC) experiment ~~is currently being~~<sup>was</sup> conducted at the Grimsel Test Site (GTS) ~~in~~<sub>in</sub> Switzerland, with the objective of improving our understanding of the aforementioned HM-coupled processes in a moderately fractured crystalline rock mass. The ISC experiment activities aim to support the development of EGS technology by 1) advancing the understanding of fundamental processes that occur within the rock mass in response to relatively large-volume fluid injections at high pressures, 2) improving the ability to estimate and model induced seismic hazard and risk, 3) assessing the potential of different injection protocols to keep seismic event magnitudes below an acceptable threshold, 4) developing novel monitoring and imaging techniques for pressure, temperature, stress, strain and displacement as well as geophysical methods such as ground-penetrating radar (GPR), passive and active seismics and 5) generating a high-quality benchmark dataset that facilitates the development and validation of numerical modelling tools.

This paper presents a literature review that highlights key research gaps concerning hydraulic reservoir stimulation, and discusses which of the aforementioned research questions can be addressed in our decameter underground stimulation experiment. We then provide an overview of the ISC project that describes the geological site conditions, the different project phases and the monitoring program.

## 2 Literature review

### 2.1 Stimulation ~~process~~<sup>by</sup> hydraulic shearing

The concept of mining heat from hot, low permeability rock at great depth was first proposed at Los Alamos National Labs in the 1970s and was called Hot Dry Rock system (Brown et al., 2012). They initially ~~envisaged~~<sup>envisioned</sup> creating a reservoir by applying oil and gas reservoir hydrofracture technology to build a heat exchanger between two boreholes. Subsequent field tests have demonstrated that hydraulic stimulation injections are effective in enhancing the permeability of a rock mass by several orders of magnitude by producing irreversible fracture

opening, whilst also increasing the connectivity of the fracture network (Kaieda et al., 2005, Evans et al., 2005b; Häring et al., 2008). Two different 'end-member' mechanisms commonly appear in discussions of permeability creation processes through hydraulic injections: 1) hydraulic fracturing as the initiation and propagation of [new](#) tensile fractures and 2) hydraulic shearing, i.e., the reactivation of existing discontinuities in shear with associated irreversible dilation that is often referred to as the self-propping mechanism. Hydraulic shearing is of particular relevance for EGS as it has been shown that slip along fractures can generate a permeability increase by up to 2-3 orders of magnitude (Jupé et al., 1992, Evans et al., 2005a; Häring et al., 2008). If the rock mass in the reservoir is stressed to a critical level (e.g., Byerlee 1978), then a relatively small reduction of effective normal stress would be sufficient to cause shearing along pre-existing discontinuities that are optimally-oriented for failure (Hubbert and Rubey, 1959; Rayleigh et al., 1976; Zoback and Harjes 1997; Evans et al., 1999; Evans, 2005). Thus, shearing and the associated permeability enhancement can occur at large distances from the injection point, even though the causal pressure increases may be low (Evans et al., 1999; Saar and Manga, 2003; Husen et al., 2007). In contrast, hydraulic fracture initiation and propagation (i.e., the original concept of EGS to connect two boreholes) requires high pressures exceeding the minimum principal stress to propagate hydro-fractures away from the wellbore. The high pressure in the fracture may interact with natural fractures and stimulate them, leading to leak-off (i.e., the extent of hydro-fractures is influenced by pressure losses and the existence of pre-existing fractures). Therefore, hydraulic fracturing is often only considered relevant in the near-field of a wellbore, where it improves the linkage between the borehole and the natural fracture system. Rutledge et al., (2004) showed that shear activation of existing fractures and creation of new fractures can occur concomitantly, dependent on the in-situ stress conditions, injection pressure, initial fracture transmissivity, fracture network connectivity and fracture orientation (e.g., McClure and Horne, 2014). Regardless of which process is dominant, the direction of reservoir growth, and therefore, the geometry of the stimulated volume, depends to a considerable degree on the in-situ stress gradient, stress orientation and the natural fracture network.

Pressurized fractures may open due to a reversible compliant response to pressure (Rutqvist 1995; Rutqvist and Stephansson 2003; Evans and Meier, 2003), or due to largely irreversible shear dilation (Lee and Cho 2002; Rahman et al., 2002). As a consequence of the coupling between pressure, fracture compliance and permanent fracture aperture changes, the pressure field does not propagate through the reservoir as a linear diffusive field, but rather as a pressure front (Murphy et al., 2004). The fracture normal and shear dilation that occurs in response to

elevated fluid pressure thus has a major influence on the magnitude and profile of the propagating pressure perturbation in the rock mass during hydraulic stimulations (Evans et al., 1999; Hummel and Müller, 2009). As a consequence, fracture compliance and normal/shear dilation characteristics have an impact on the size and geometry of the reservoir created during hydraulic stimulation.

Although the aforementioned processes are conceptually well understood, the quantification and detailed understanding required for designing stimulations and truly engineering geothermal reservoirs are insufficient. There remains considerable uncertainty as to how the above processes interact, and what rock mass characteristics and injection metrics control the dominant mechanisms (Evans et al, 2005a; Jung 2013). Thermo-hydro-mechanically coupled numerical models have become widely used for analysing relevant aspects of reservoir stimulation in retrospective (e.g., Baujard and Brueel, 2006; Rutqvist and Oldenburg 2008; Baisch et al., 2010; Gischig and Wiemer, 2013) or as prospective tools for predicting reservoir behaviour or alternative stimulation strategies (e.g., McClure and Horne 2011; Zang et al., 2013; Gischig et al., 2014; McClure 2015; Yoon et al., 2015). The fact that such numerical models must be parameterized from sparse quantitative field-scale data is a major limitation of all those studies. In the following we present an overview of the experimental observations of hydro-mechanical coupling that are relevant to the parameterization of numerical models. These stem from reservoir-scale (i.e., hectometre) stimulation operations, such as in EGS demonstration projects or oil and gas reservoirs, intermediate-scale (i.e., decametre) in-situ-experiments, and small-scale laboratory experiments.

#### 2.1.1 Reservoir-scale experiments

The paucity of high-quality data on the stimulation process from reservoir-scale projects is largely ~~because they tend to be conducted at depths~~ a results of the considerable depth of typical geothermal resources (e.g., several kilometres), which prohibits the observation of hydro-mechanical processes from instrumentation installed within the reservoir. In the geothermal domain, such projects constitute expensive experiments and thus are relatively few in number, whereas, in the oil and gas domain, where hydrofracture operations are frequent and routine, the data tend to be proprietary. Nevertheless, some notable datasets have been acquired for deep brine injection projects (Ake et al., 2005; Block et al., 2015), deep scientific drilling projects such as the German KTB project (Zoback and Harjes 1997; Emmermann and Lauterjung 1997; Jost et al., 1998; Baisch and Harjes 2003), hydraulic fracturing for oil & gas production

enhancement (Warpinski 2009; Das and Zoback 2011; Dusseault et al., 2011; Pettitt et al., 2011; Vermilyen and Zoback 2011; Boroumand and Eaton 2012; van der Baan et al., 2013; Bao and Eaton 2016;), and during the stimulation of deep geothermal boreholes (Parker, 1989; Jupe et al., 1992; Cornet & Scotti, 1993; Tezuka & Niitsuma, 2000; Asanuma et al., 2005; Evans et al., 2005a; Häring et al., 2008; Brown et al., 2012; Baisch et al., 2015; ). Well-documented hydraulic stimulation datasets generally include microseismic observations as well as injection pressures and flow rates and occasionally, tilt monitoring (Evans, 1983; Warpinski et al., 1997). Although much information can be gained from these datasets, including imaging of microseismic structures (Niitsuma et al. 1999; Maxwell, 2014), energy balance between injected fluids and seismic energy release (Boroumand and Eaton 2012; Zoback et al., 2012; Warpinski et al., 2013), and source mechanisms (Jupe et al., 1992; Deichmann and Ernst, 2009; Warpinski and Du 2010; Horálek et al, 2010), the constraints placed on the processes are insufficient to resolve details of the hydro-mechanical processes that underpin permeability enhancement, flow-path linkage, channelling, or the interaction with natural fractures. Many of these processes possibly also depend on rock type. For instance, case studies analysed by Evans et al., (2012) support the notion that injection into sedimentary rock tends to be less seismogenic than in crystalline rock. Moreover, it is likely that a significant part of the permeability creation processes take place in an aseismic manner (Cornet et al., 1997; Evans et al., 1998; Guglielmi et al., 2015b; Zoback et al., 2012), implying that seismic monitoring may only illuminate parts of the stimulated rock volume. In many deep hydraulic stimulation projects the rock mass is only accessed by one or at most a few boreholes, and the structural and geological models of the reservoir are not well defined. In general, the displacements on fractures arising from the injection can only be directly measured where they intersect the boreholes, and deformation occurring within the rock mass is poorly resolved.

Despite limitations in reservoir characterization and monitoring, significant insights into the stimulation process can be gleaned from the experience from the EGS projects that have been conducted to date. Two examples in crystalline rock are studies of stimulation-induced fault slip and changes of flow conditions in the fracture network associated with the permeability creation processes at the Soultz-sous-forêt (Cornet et al., 1997; Evans et al., 2005b) and the Basel EGS projects (Häring et al., 2008). At both sites, it has been shown that permeability in the near-wellbore region increased by 2-3 orders of magnitude. At Basel, a single initially-impermeable fracture has been shown to take at least 41% of the flow during the 30 l/s injection stage (Evans and Sikaneta, 2013), whereas at Soultz-sous-forêt, the stimulation of the 3.5 km deep reservoir served to enhance the injectivity of a number of naturally-permeable fractures



(Evans et al., 2005b). These fractures tended to be optimally oriented for fault slip, as also found elsewhere by Barton et al. (1995, 1998) and Hickman et al. (1998). At Soultz-sous-forêt, it was possible to estimate stimulation-induced slip and normal opening of fractures that cut the borehole by comparing pre- and post-stimulation acoustic televiewer logs (Cornet et al., 1997; Evans et al., 2005). Shearing of fractures was also proposed as the predominant mechanism of permeability enhancement [in granite](#) at the Fjällbacka site in Sweden, by Jupe et al. (1992), based upon focal mechanism analysis. The above observations provide evidence of a link between shearing and permeability changes.

An additional, important lesson from deep stimulation projects is that the stress conditions in reservoirs may be strongly heterogeneous, and that this influences the flow field (e.g., Hickman et al., 2000). For instance, profiles of horizontal stress orientation defined by wellbore failure observations commonly show significant fluctuations whose amplitude varies systematically with scale (Shamir and Zoback, 1992; Valley and Evans 2009; Blake and Davatzes, 2011), even though that may have an average trend consistent with the tectonic stress field. Strong deviations may occur in the vicinity of faults, indicating past fault slip and complex fault zone architecture (Valley and Evans, 2010; Hickman et al., 2000). Similarly, the hydro-mechanical properties of faults depend on the fault architecture, which itself depends on lithology and the damage history accumulated over geological time (Caine et al., 2006, Faulkner and Rutter 2008; Guglielmi et al., 2008, Faulkner et al., 2010, Jeanne et al., 2012). Within a fault zone, permeability and compliance contrasts can vary by several orders of magnitude (Guglielmi et al., 2008), thus complicating the predictability of hydro-mechanical responses to stimulations. In some EGS projects, it was observed that the hydraulic communication between injection and production boreholes may be unsatisfactory for efficient exchange of heat, either because of high flow impedance, such as [in granite rock](#) at Ogachi, Japan, (Kaieda et al., 2005), or because of flow channelling, as inferred from early thermal drawdown [in granitic rock](#) at Rosemanowes, UK (Nicol and Robinson, 1990), and [in granodiorite at](#) Hijiori, Japan (Tenma et al., 2008).

#### 2.1.2 Laboratory-scale experiments

On the laboratory-scale, considerable effort has been devoted to experiments that address the role of effective stress changes on normal fracture opening and closure, shear dilatancy and related permeability changes (Goodman 1974; Bandis et al., 1983; Yeo et al., 1998; Esaki et al., 1999; Gentier et al., 2000; Olson and Barton, 2001; [Samuelson et al., 2009](#)). These experiments have demonstrated that the relationships between fluid pressure change, fracture

opening and flow within rough natural fractures are strongly non-linear. Even though significant progress has been made on defining permeability changes during normal opening and shear slip on the laboratory scale, the non-linear relationships between fracture opening, changes in effective normal stress, shearing, and the resulting permeability are yet not well constrained (Esaki et al., 1991; Olsson et al., 2001, Vogler et al., 2015). One common approach is to represent the fracture as two parallel plates whose separation, the hydraulic aperture, gives the same flow rate per unit pressure gradient as would apply for the natural fracture. For parallel plates and laminar flow, the flow rate per unit pressure gradient is proportional to the cube of hydraulic aperture. However, for rough-walled fractures, the hydraulic aperture,  $a_h$ , is generally only a fraction of the mean mechanical aperture,  $a_m$  (i.e., the mean separation of two surfaces), the fraction tending to decrease with smaller apertures, although the precise relationship is difficult to derive from fracture geometry alone (Esaki et al., 1999; Olsson and Barton 2001; Vogler et al., 2015). At larger mechanical apertures, limited evidence suggests that an incremental form of the cubic law might hold such that changes in mechanical aperture give rise to equal changes in hydraulic aperture, at least for normal loading (e.g., Schrauf and Evans, 1986; Evans et al. 1992; Chen et al., 2000). For shear-induced dilation, an additional complication arises from channel clogging due to gouge production (e.g., [Lee et al., 2002](#)), [Lee et al., 2002](#)). [Particle transport through fluid flow \(Candela et al., 2014\) and mineralogy \(Fang et al., 2017\) may additionally influence permeability changes in a complex manner.](#) Deviations from the cubic law also occur when flow becomes non-laminar, which tends to occur at high flow velocities (Kohl et al., 1997), or at feed points in boreholes (e.g., Hogarth et al., 2013; Houben, 2015).

Dilatancy associated with shearing is often expressed in terms of a dilation angle, which is a property describing the relationship between mean mechanical aperture and slip. Dilation angle depends on the fracture surface characteristics, the effective normal stress and the amount of slip. Particularly important within the stimulation context is the dependence of dilation on effective normal stress, the dilation angle tending to decrease at higher effective normal stress, in large part because shorter wavelength asperities are sheared off (Evans et al., 1999). Thus, shearing-induced dilation is likely to be more effective at low effective normal stress, such as in the near field of the injection where fluid pressures are relatively high. Clearly, insights from laboratory experiments into the relationships describing fracture dilation and permeability changes are important for understanding field observations in EGS reservoirs (e.g., Robinson and Brown; 1990; [Elsworth et al., 2016; Fang et al., 2018](#)), and also for parametrizing numerical models.

328

### 329 2.1.3 Intermediate-scale experiments

330 In-situ experiments at the intermediate-scale (i.e., decameter-scale) serve as a vital bridge  
331 between laboratory and reservoir scales. As such, they can contribute to an improved  
332 understanding of reservoir behaviour during stimulation, and to enable up-scaling of hydro-  
333 mechanical information obtained from laboratory experiments (Jung, 1989; Martin et al., 1990;  
334 Rudquist, 1995; Schweisinger et al., 1997; Cornet et al., 2003; Murdoch et al., 2004, Cappa et  
335 al., 2006; Derode et al., 2013; Guglielmi et al., 2014; 2015). Much experience has been gained  
336 from stress testing using the hydraulic methods of hydro-fracturing (HF), hydraulic testing of  
337 pre-existing fractures (HTPF) (Haimson and Cornet, 2003), and hydro-jacking (Evans and  
338 Meier, 1995; Rutqvist and Stephansson, 1996). Hydraulic tests have been commonly used to  
339 quantify pressure-sensitive permeability changes (Louis et al., 1977), and normal stiffness in  
340 natural fractures or faults (Rutqvist et al., 1998). Evans and Wyatt (1984) estimated the closure  
341 of a fracture zone from observed surface deformations induced by drilling-related drainage of  
342 fluid pressure within the structure. Similarly, Gale (1975), Jung (1989), Martin et al. (1990),  
343 Guglielmi et al (2006), and Schweisinger et al. (2009) used borehole caliper sondes to monitor  
344 changes in fracture aperture and pressure during hydraulic jacking tests. The resulting  
345 displacements and the flow and pressure responses allowed relationships between mechanical  
346 and hydraulic aperture changes to be established and helped to constrain the fracture/fault  
347 normal compliance at larger scales.

348 Irreversible permeability increases arising from slip-induced dilation of natural fractures are  
349 particularly relevant for stimulation of EGS and hydrocarbon reservoirs. To study the  
350 phenomenon in-situ, Guglielmi et al. (2014) developed a novel double packer system (SIMFIP)  
351 that allows the simultaneous measurement of pressure, flow rates and 3-dimensional relative  
352 displacements occurring across a fracture isolated within the interval in response to injection.  
353 The device was successful in reactivating a fault zone in a limestone formation in Southeast  
354 France (Derode et al., 2013; Guglielmi, et al., 2015). Pressure, injection rate and 3D  
355 displacements in the SIMFIP interval were measured, together with microseismic activity, tilt  
356 and fluid pressure in the vicinity of the injection borehole. The dataset is unique, and provided  
357 quantitative insights into the relationships between (i) fault dislocation including shear and  
358 permeability changes, (ii) fault normal compliance and static friction, and (iii) slip velocities  
359 and magnitudes and their relation to aseismic and seismic slip. Recently, a similar experiment  
360 was conducted in a series of interacting complex fault zones in shale (Guglielmi et al., 2015).

Distributed pore pressure and strain sensors across the faults allowed the evolution of the pressurized and slipped areas to be constrained, which was not previously possible. Such experiments provide a useful methodology for advancing our understanding of the hydro-mechanical coupled processes in complex faults.

## 2.2 Hydraulic stimulation by hydraulic fracturing experiments

Experience gained from large scale stimulation of EGS reservoirs in crystalline rock suggests that hydraulic shearing is the dominant mechanism for permeability creation, at least remote several tens of meters distance from the injection point (e.g. Evans, 2014). However, the initiation and propagation of hydraulic fractures may be an important mechanism in the near field of the wellbore to connect the wellbore to the pre-existing fracture network in the reservoir (Cornet and Jones, 1994). Considerable effort has been devoted to understand the initiation and propagation of hydraulic fractures on both the laboratory and intermediate field scale.

### 2.2.1 Laboratory scale hydraulic fracturing experiments

Many well-controlled, small-scale laboratory experiments on hydrofracture are documented in the literature (Jaeger 1963; Zoback et al., 1977; Warpinski et al., 1982; Bruno and Nakagawa 1991; Johnson and Cleary 1991; Song et al., 2001; Jeffrey and Bunger 2007; Bunger et al., 2011). For such experiments, samples of various shapes (e.g., hollow cylinders and perforated prisms) are loaded along their boundaries and the internal fluid pressure is increased until a hydraulic fracture initiates and propagates. For some tests, transparent material like polymethylmethacrylate (PMMA) were used to image fracture growth. Some experimental setups include multi-material "sandwiches" to study the effect of stress contrast on hydraulic fracture containment (Jeffrey and Bunger 2007; Warpinski et al., 1982). Others study the interaction of propagating hydrofractures with pre-existing fractures (Zoback et al., 1977; Meng, 2011; Hampton et al, 2015) or rock textures (Ishida 2001; Chitrala et al., 2010), the impact of injection fluids with different viscosities (Bennour et al., 2015) or the role of stress anisotropy (Doe and Boyce, 1989) on the geometry and orientation of generated fractures, or the interaction between multiple fractures (Bunger et al., 2011). These laboratory studies provide important results relevant for EGS. For instance, in the common situation where a family of natural fractures is not normal to the minimum principal stress, injections with high viscosity fluids (viscosity dominated regime) may help maintain tensile fracture propagation normal to the minimum principal stress despite the presence of cross-cutting fractures (Zoback

et al., 1977), whereas low viscosity fluids (toughness dominated regime) such as water will promote leak-off into the cross-cutting natural fractures, whose permeability may be increased by shear (Rutledge et al, 2003). This leak-off will tend to limit hydrofracture propagation. Laboratory studies also give insights into the influence of shear stress shadow and transfer on hydraulic fracture growth (Bunger et al., 2011). Laboratory tests have also been essential for providing well-controlled fracture initiation and propagation datasets to benchmark hydraulic fracture simulation codes (Bunger et al., 2007).

#### 2.2.2 Intermediate scale hydraulic fracturing experiments

Intermediate scale experiments have been performed to study initiation and propagation of hydraulic fractures. Typically, they are conducted from boreholes drilled from excavations to facilitate dense near-field instrumentation and secure good experimental control. An early example is the series of experiments that took place at the Nevada Test Site in soft, bedded volcanic tuff with high porosity and high permeability (Warpinski, 1985; Warren and Smith, 1985). The pressure, flow and fracture aperture were monitored during the experiments, and the fractures were mined back at the end of the experiments. The mine back revealed that stress contrasts were the predominant influence on hydraulic fracture containment, and that the fractures consisted of multiple fracture strands and thus differed significantly from simple shapes assumed in theoretical studies. This complexity of the fracture shape impacts the flow and pressure distribution within the propagating hydraulic fractures. Another notable series of in-situ tests on hydraulic fracture propagation within the context of coal-seam mining and block cave mine preconditioning have been performed by the hydraulic fracture group of CSIRO (Chacón et al., 2004; Jeffrey et al., 1993; 1992, 2009; Jeffrey and Settari 1995; van As et al., 2004; van As and Jeffrey 2002, 2000). The block cave mining experiments were performed in hard rock media and thus are the more relevant to EGS. Those conducted in the quartz monzonite porphyries at the Northparkes mine in Australia are probably the most detailed and densely instrumented tests executed to date, and included tiltmeter monitoring, a micro-seismic network, and pore pressure sensors as well as detailed rock mass and stress characterization- (Jeffrey et al., 2009). Hydrofractures were formed with water and cross-linked gels, with coloured plastic proppants added in order to facilitate their identification once the test volume was mined back. The mapped trajectories of the hydraulic fractures exhibited complex geometries, sometimes with multiple branching and crossing of joints, veins and shear zones, with and without offset. Sub-parallel propped sections accounted for 10 to 15% of the total

fracture extent, which microseismic activity indicated was more than 40 m from the injection point. The results demonstrate that the geometry of the fractures is much more complex than typically obtained in small scale laboratory experiments in a homogeneous material and uniform stress field. The complexity close to the injection point is controlled by the near-well stress perturbation and the interaction with natural fractures and rock mass fabric.

Natural fractures have also a strong influence on the propagation of hydraulic fractures. The propagation regime (i.e., viscosity-dominated or toughness-dominated (Detournay, 2016)) can be controlled by the injection rate and injected fluid rheology and will have likely a strong influence on the interaction with natural fractures and the final complexity of the hydraulic fractures, although this has not been validated by in-situ experiment. Another relevant aspect that has not been investigated with in-situ tests is the problem of proppant transport and distribution within the created fractures. Indeed, in the case of hydraulic fractures, the self-propping mechanism, which results in a permanent aperture increase, is unlikely to be effective, and so proppant placement is necessary for insuring permanent permeability enhancement. Finally, the nature of the microseismicity generated by hydraulic fracturing is not adequately understood. Moment tensor analyses can offer insight into the nature of the failure in a microseismic event (Warpinski and Du, 2010; Eyre and van der Baan, 2015). For example, they can help resolve whether the seismic radiation is primarily generated by shear on pre-existing fractures that are intersected by the propagating fracture, with relatively little energy generated by the advancing mode I tip of the hydraulic fracture (Sileny et al, 2009; Horálek et al, 2010; Rutledge et al., 2004).

### 2.3 Rock mass deformation and stress interaction

Injection of fluid into a rock mass invariably leads to deformation of the surrounding rock mass due to poroelasticity (Biot 1941) or slip-related stress changes (McClure and Horne 2014). Numerical studies have suggested that stress interaction between adjacent fractures can have a significant impact on the stimulation results (e.g., Preisig et al., 2015; Gischig and Preisig 2015). In most reservoir stimulations, the microseismic clouds exhibit an oblate shape, due primarily to the interaction between the strongly anisotropic stress field with the natural fracture population. This tendency to form an oblate ellipsoidal shape instead of a sphere may also be promoted by stress transfer from slipped fractures which tends to inhibit slip on neighbouring fractures (Gischig and Preisig 2015). Schoenball et al. (2012) and Catalli et al. (2013) have demonstrated that induced earthquakes preferably occur where stress changes generated by

preceding nearby earthquakes render the local stress field to be more favourable for slip. Similar effects have been observed for natural earthquakes (Stein 1999). The effect becomes more important during stimulation as time goes on, especially at the margin of the seismicity cloud. Direct observation of deformation associated with fluid injection has been observed in several intermediate-scale in-situ experiments. Evans and Holzhausen (1983) report several case histories of using tiltmeter arrays to observe ground deformation above high pressure hydraulic fracturing treatments. The results show clear evidence of self-propping of the induced fractures. van As et al. (2004). Jeffrey et al (2009) used a tiltmeter array to monitor a hydrofracturing treatment at the Northparkes mine in Australia. The pattern of tilting indicated the induced fracture was sub-horizontal, which was confirmed by excavating the fracture traces. Evans and Wyatt (1984) modelled strains and tilts occurring around a well during air drilling and found the deformation was due to opening of a pre-existing fracture zone in response to fluid pressure changes. Derode et al. (2013) observed tilts of  $10^{-7}$ - $10^{-6}$  radians some meters away from small volume injections into a fault in limestone. In contrast, Cornet and Deroches (1990) monitored surface tilts with a 6 instrument array during injections of up to 400 m<sup>3</sup> of slurries into granite at 750 m depth at the Le Mayet test site in France and report no resolved signal associated with the injections.

Rock mass deformation during stimulation injections necessarily leads to stress changes in the rock mass. Small but non-zero residual stress changes induced by hydraulic fracturing were measured using a stress cell by van Assa et al. (2004). Stress changes during injections are recognized as playing a potentially important role in determining the pattern of fracture and slip that develops during the injection (e.g., Preisig et al., 2015; Catalli et al, 2013).

## 2.4 Seismic and aseismic slip

A significant fraction of the slip that occurs on fractures within a reservoir undergoing stimulation may be aseismic, depending upon in-situ stress and geological conditions. That aseismic slip has occurred is often inferred indirectly from changes in the hydraulic characteristics of a reservoir without attendant micro-seismicity (Scotti and Cornet 1994; Evans, 1998). Direct detection of aseismic slip is difficult as it requires relative displacements across fractures to be resolved from borehole or near-field deformation measurements (e.g., Maury 1994; Cornet et al., 1997, Evans et al., 2005b). For example, Cornet et al. (1997) compared borehole geometry from acoustic televiewer logs run before and after the 1993 stimulation at the Soultz-sous-forêt site and found that 2 cm of slip had apparently occurred

493 across a fracture. The cumulative seismic moment of events in the neighbourhood of the  
494 fracture was insufficient to explain the observed slip magnitude, thereby suggesting a large  
495 portion of the slip had occurred aseismically. Indeed, almost all fracture zones that were  
496 hydraulically active during the stimulation showed evidence of shear and opening-mode  
497 dislocations of millimetres to centimetres (Evans et al., 2005b).

498 The transition from aseismic to seismic slip was directly observed by Guglielmi et al. (2015)  
499 during fluid injection into a well-instrumented fault in limestone in a rock laboratory at 280 m  
500 depth. Some 70% of a 20-fold permeability increase occurred during the initial aseismic slip  
501 period. The transition to seismic slip coincided with reduced dilation, and the inference that slip  
502 zone area exceeded the pressurized area, suggesting the events themselves lay outside the  
503 pressurized zone. Modelling the observed slip as occurring on a circular fracture with total  
504 stress drop gave a radius of 37 m and a moment release of  $65 \times 10^9$  Nm, far larger than the estimated  
505 seismic moment release of the order of  $10^6$  Nm, again indicating most slip was aseismic.  
506 Guglielmi et al. (2015) concluded that the aseismic behaviour is due to an overall rate-  
507 strengthening behaviour of the gauge filled fault and seismicity occurs due to local frictional  
508 heterogeneity and rate-softening behaviour. These results are consistent with laboratory  
509 experiments performed by Marone and Scholz (1988) on fault gauge which suggest that slip at  
510 low effective normal stresses (as anticipated in the near field of a high-pressure injection) and  
511 within thick gouge layers tends to be stable (aseismic).

512 Apart from these observations, aseismic slip has been mostly discussed from the perspectives  
513 of semi-analytical or numerical models. Garagash and Germanovic (2012) used a slip-  
514 weakening model to show that aseismic slip depends on the stress conditions and injection  
515 pressure. Zoback et al. (2012) used McClure's (2012) rate-and-state friction model to show that  
516 aseismic slip becomes more prominent for stress states farther from the failure limit. Using the  
517 same model, Gischig (2015) demonstrated that slip velocity depends on fault orientation in a  
518 given stress field. For non-optimally oriented faults, aseismic slip becomes more prominent and  
519 the seismicity is less pronounced for lower slip velocities and shorter rupture propagation  
520 distances. These model results suggest that aseismic slip and low slip velocities may be  
521 promoted by avoiding the stimulation of optimally oriented critically-stressed faults. Clearly, a  
522 more detailed understanding of the conditions that result in aseismic slip may be a basis for less  
523 hazardous stimulations.



## 2.5 Induced seismicity

Keeping induced seismicity at levels that are not damaging or disturbing to the population continues to be a major objective for EGS (Giardini, 2009; Bachmann et al., 2011; Majer et al., 2012; Evans et al., 2012) and other underground engineering projects (oil and gas extraction, liquid waste disposal, gas and CO<sub>2</sub> storage). Man-made earthquakes are not a new phenomenon (Healy et al. (1968), McGarr, 1976; Pine et al., 1987; Nicholson and Wesson, 1990, Gupta, 2003). However, the occurrence of several well-reported felt events near major population centres has served to focus attention on the problem (Giardini, 2009; Ellsworth 2013; Davies et al., 2013; Huw et al., 2014; Bao and Eaton, 2016). Some even led to infrastructure damage, such as followed the Mw5.7 event in Oklahoma, USA (Keranen et al., 2013), or the suspension of the projects (e.g., the geothermal projects at Basel (Häring et al., 2008) and St. Gallen (Edwards et al., 2014) in Switzerland. As a consequence, a substantial research effort has been initiated to understand the processes that underlie induced seismicity. Examples are the numerous studies that have been performed using the high-quality seismic dataset collected during the Basel EGS experiment. Dyer et al. (2010), Kraft and Deichmann (2014) and Deichmann et al. (2014) analysed waveforms of the seismicity to determine reliable source locations. Terekawa et al. (2013) used an extended catalogue of the focal mechanism solutions of Deichmann and Ernst (2009) to estimate the stress field at Basel and to infer the pore pressure increase required to trigger the events. Goertz-Allmann et al. (2011) determined stress drop for the Basel seismicity and found higher stress drops at the margin of the seismic cloud than close to the injection borehole. A similar dependency for Gutenberg-Richter b-values was found by Bachmann et al. (2012) – lower b-values tended to occur at the margin of the seismicity cloud and at later injection times.

There are numerous analyses of induced seismicity at other EGS sites. Pearson (1981) and Phillips et al (1997) analysed microseismicity generated during the stimulation of the 2930 m deep ‘large Phase 1’ and the 3460 m deep Phase 2 reservoirs respectively at the Fenton Hill EGS site, New Mexico. Bachelor et al. (1983) and Baria and Green (1986) summarize microseismicity observed during the stimulation injections into the Phase 2a and 2b reservoirs at Rosemanowes in Cornwall, UK. Tezuka and Niitsuma (2000) examined clusters of microseismic events generated during the stimulation of the 2200 m deep reservoir at the Hijiori EGS site in Japan. Baisch et al. (2006, 2009, 2015) analysed data from different stages of the stimulation of the Habanero EGS reservoir in the Cooper Basin, Australia. Calò et al. (2011) used microseismicity generated during the stimulation of the 5 km deep EGS reservoir at Soultz-sous-forêt to perform time-lapse P-wave tomography to infer pore pressure migration

during injection. [Various authors also explored the vast induced seismicity dataset of >500'000 events recorded since the 1960s at the Geysers geothermal site, where recently also an EGS demonstration stimulation has been performed \(Garcia et al., 2012; Jeanne et al., 2014\). The observed seismicity was partly related to injections \(Jeanne et al., 2015\) and thermo-elastic stress changes \(Rutqvist and Oldenburg, 2008\). Here, local variability in the stress field \(Martínez-Garzón et al., 2013\) and volumetric source components \(Martínez-Garzón et al., 2017\) were inferred from detailed analysis of injection-induced seismicity.](#)

Another major focus of induced seismicity research has been the development of hazard assessment tools for injection related seismicity. The primary goal of these efforts is to develop a dynamic, probabilistic and data-driven traffic light system that can provide real-time hazard estimates during injections (Karvounis et al., 2014; Kiraly et al., 2016), as opposed to the traditional, static traffic light system (Bommer et al., 2006). Bachmann et al. (2011) and Mena et al. (2013) developed several statistical models and tested them in pseudo-prospective manner using the Basel seismicity dataset. More complex models including physical considerations and stochastic processes (so-called hybrid-models) were developed to include information on the reservoir behaviour and from the spatio-temporal evolution of seismicity (Goertz-Allmann and Wiemer, 2013; Gischig and Wiemer, 2013; Kiraly et al., 2016). Mignan et al. (2015) evaluated reported insurance claims arising from the Basel induced seismicity in order to infer procedures for evaluating risk based on induced seismic hazard estimates.

The Gutenberg-Richter b-value, which describes the reduction in the frequency of occurrence of events with increasing earthquake magnitude, plays a key role in induced seismic hazard analysis. Schorlemmer et al. (2005) examined the b-values of earthquakes in different stress regimes and found lower values correlated with areas of higher differential stress. Similar trends have been reported for induced seismicity (Bachmann et al., 2012), but also in tectonic earthquakes (Tormann et al., 2014; Torman et al., 2015; Spada et al., 2013) and laboratory experiments (Amitrano 2003; Goebel et al., 2012). Thus, it was hypothesized that b-values are related to local stress conditions (Scholz, 2015), or - in the context of induced earthquakes – to a combination of pressure and stress conditions. Considering standard scaling laws between magnitudes and earthquake source dimensions (i.e., slip and slipped area), it has to be expected that seismicity with high b-values may have an indirect but strong impact on permeability enhancement (Gischig et al., 2014). However, these observations have so far only been qualitatively established, as the absolute stress state within the rock volume that hosts the seismicity whose b-value is estimated has not been quantitatively determined.

Whilst the hazard associated with induced seismicity is clearly an important factor for reservoir engineering, it should not be forgotten that the shearing of fractures and fracture zones, which is the source of the seismicity, is a key process in the irreversible permeability enhancement that is the objective of the stimulation injections. Furthermore, precise mapping of the 3-D distribution of events provides an indication of the direction of fluid pressure propagation and hence the geometry (i.e., size, shape, degree of anisotropy) of the distribution of permeability enhancement – information that is vital for drilling subsequent well (Niitsuma et al., 1999). Managing induced seismic hazard also requires considering the design of reservoir attributes such as size, system impedance, and heat exchanger properties that control system longevity (e.g., Gischig et al., 2014). Currently, few case studies consider both seismicity and the related changes that occurred in the reservoir (e.g., Evans et al., 2005a), and relatively few studies even report both permeability changes or well injectivity (e.g., Häring et al., 2008; Evans 2005b; Kaieda et al., 2005; Petty et al., 2013). More work is needed to quantitatively link the spatial, temporal or magnitude distribution of seismicity with the thermo-hydraulic-mechanical properties of the rock mass under stimulation conditions. We believe controlled experiments on the intermediate (in-situ test site) scale supported by laboratory-scale experiments could be key in making progress towards this end.

## 2.6 Open research ~~question~~questions in hydraulic stimulation research

Research on reservoir stimulation for deep geothermal energy exploitation has been largely performed through laboratory observations, large-scale projects, and numerical models. Observations of full-scale reservoir stimulations have yielded important observations. However, the difficulty in observing the processes occurring within the reservoir under stimulation conditions severely limits the understanding of the permeability creation processes in a way that aids future stimulation design.

Laboratory experiments are attractive because they are controllable and readily repeatable, but they suffer from two main limitations: 1) Upscaling results to the field-scale is affected by large uncertainties (Gale 1993). Although there is evidence that the roughness of fresh fracture surfaces obeys well-defined scaling over many orders of magnitude (Power and Tullis, 1991; Schmittbuhl et al., 1995), complications arise in upscaling the aperture distribution and hence permeability of two semi-mated rough surfaces due to the effects of damage and wear of the asperities during shearing and gouge formation (Amitrano and Schmittbuhl, 2002; Vogler et al, 2016). 2) Laboratory tests are typically performed on single fractures in relatively homogeneous

625 materials and uniform stress conditions, which makes upscaling to structures with multiple  
626 fractures such as fracture zones challenging. Similarly, hydraulic fracture propagation  
627 behaviour is usually studied with homogenous rock samples under uniform stress, and this can  
628 lead to an over-simplistic fracture flow and/or hydraulic fracture propagation behaviour. In an  
629 EGS reservoir, for example, the stress may be heterogeneous on the meter to decametre-scale  
630 (Evans et al., 1999; Valley and Evans 2009; Blake and Davatzes, 2011), and the rock mass may  
631 contain various heterogeneities such as stiffness contrasts, fractures or faults (Ziegler et al.,  
632 2015).

633 Because of the large uncertainties in upscaling, many numerical studies make direct (i.e., not  
634 upscaled) use of laboratory results to parameterize HM-coupled models for EGS, because so  
635 few field-scale relationships are available (e.g., Rutqvist, 2011; McClure, 2012; Gischig et al.,  
636 2014). This impacts the reliability of the numerical simulation studies, because the descriptions  
637 of the processes and the input parameter values may be inappropriate for the scale of the  
638 simulation.

639 Clearly there is a need for field-scale hydraulic stimulation experiments that bridge the various  
640 scales, and are performed with the target rock mass equipped with a comprehensive monitoring  
641 system to capture details of the processes. Recently several intermediate-scale hydro-shearing  
642 and hydrofracturing experiments have been performed in a densely instrumented rock mass  
643 (i.e., Guglielmi et al., 2008, 2014 and 2015; Jeffrey et al., 2009). The hydro-shearing  
644 experiments by Guglielmi et al. (2008) have all been in sedimentary rock types at shallow depth.  
645 No such densely-instrumented experiments have been performed in fractured and faulted  
646 crystalline basement rocks faults, the target rocks for most EGS, where a variety of complex  
647 fault architectures and stress-fracture system configurations need to be investigated. The ~~on-~~  
648 ~~going~~ In-situ Stimulation and Circulation (ISC) experiment ~~tries to contribute to the filling of~~  
649 ~~this addresses these~~ research gap. ~~In particular, the experiment addresses gaps, with a focus on~~  
650 the following research questions: (RQ):

- 651 [RQ 1] What is the relationship between pressure, effective stress, fracture aperture, slip,  
652 permeability and storativity? (i.e., the hydro-mechanical coupled response of  
653 fractures)?  
654 [RQ 2] How does the transient pressure field propagate in the reservoir during stimulation?  
655 [RQ 3] How does the rock mass deform as a result of rock mass pressurization, fracture  
656 opening and/or slip?

- 657 [RQ 4] How does stress transfer inhibit or promote permeability enhancement and  
658 seismicity along neighbouring fractures?
- 659 [RQ 5] Can we quantify the transition between aseismic and seismic slip and the friction  
660 models (such as rate-and-state friction) describing slip evolution and induced  
661 seismicity?
- 662 [RQ 6] How do hydraulic fractures interact with pre-existing fractures and faults and how  
663 can the interaction be controlled?
- 664 [RQ 7] How does induced seismicity evolve along faults and fractures of different  
665 orientation?
- 666 [RQ 8] How does induced seismicity along stimulated faults compare to induced seismicity  
667 along newly created hydraulic fractures?
- 668 [RQ 9] Can we quantify the link between spatial, temporal and magnitude distribution of  
669 induced seismicity and HM coupled properties of fractures and faults?
- 670

### 671 3 The ISC experiment

672 The objective of the ISC experiment ~~is was established~~ to ~~contribute in finding~~ find answers to  
673 the above mentioned research questions by 1) stimulating a naturally fractured crystalline rock  
674 volume at the decameter scale that is exceptionally well characterized in terms of its structural,  
675 geomechanical, and hydraulic conditions and 2) providing a dense network of sensors within  
676 the test volume so as to establish a 3D data set at high spatial resolution that will yield detailed  
677 insight into geomechanical processes associated with induced micro-earthquakes, fracture  
678 shearing, permeability creation and fluid circulation. The experiment was planned and prepared  
679 during 2015 and 2016, and executed during two series of experiments in February and May  
680 2017. We here give a general overview of the experiment site, the main concepts, and the design  
681 of the experiment, without detailing results that are to be published in future work.

682

#### 683 3.1 The in-situ rock laboratory

684 The ISC experiment ~~is being~~ was performed at the Grimsel Test Site (GTS), near the Grimsel  
685 Pass in the Swiss Alps (Figure 1 ~~Figure 1a~~). The GTS is owned by the National Cooperative for  
686 the Disposal of Radioactive Waste (NAGRA), and was developed ~~as a facility~~ to host in-situ  
687 experiments relevant to nuclear waste repository research. The facility consists of a complex of  
688 tunnels at a mean depth of 480 m that penetrate crystalline rock with well-documented  
689 structures. The rock type is considered representative for the Alpine crystalline basement that

Formatiert: Schriftart: Nicht Kursiv

is a main target for EGS. The test site for the ISC experiment is located in the southern part of the GTS (marked in blue in [Figure 1b](#)) between a Tunnel that is called AU Tunnel in the west and the VE Tunnel in the east.

The rock at the GTS consists of Grimsel granodiorite and Central Aar granite. Both show an alpine foliation that strikes NE and dips steeply at  $\sim 77^\circ$  towards SE. The moderately fractured rock mass is intersected by ductile and brittle shear zones, as well as brittle fractures and metabasic dykes. Within the ductile shear zones, numerous fractures that are commonly partially filled with gouge are present. ~~Three shear zone orientations can be distinguished at the GTS (Keusen 1989). The S1 shear zones are parallel to the alpine foliation with an orientation of 142/77 (i.e., dip direction/dip). The S2 shear zones are slightly younger than S1 and oriented with 157/75 (Keusen et al., 1989a). Shearing of the S2 structures has led to minor folding of the S1 structures (Wehrens, 2015). The youngest shear zone direction (so called S3), have E-W strikes and southward dips (183/65), and often show evidence of dextral strike-slip movement. The target volume for the injections contains an S3 shear zone that is a fracture zone bound by two metabasic dikes on either side, and that is intersected by three ductile S1 shear zones.~~

### 3.2 Experimental Phases

The ISC experiment ~~is~~was divided into three phases (Figure 2). ~~To answer all aforementioned research questions a profound understanding of the local geology, hydrogeology, stress state and rock mass properties is essential. Thus, the~~The first phase is (2015-2016) was a pre-stimulation phase that aims to characterize the rock volume in terms of geological ~~and~~ structural ~~stress~~ conditions, the local stress state, hydraulic and thermal properties, and fracture connectivity, ~~all of which is essential for the design of the experiment and the interpretation of experimental results.~~ In addition, during the pre-stimulation phase, a monitoring system ~~is~~was established that allows capturing the seismo-hydro-mechanical response at high spatial and temporal resolution ~~that is necessary to address the outlined research questions.~~ The *second phase* (February – May 2017) - the main hydroshearing and ~~hydrofracturing~~hydrofracturing experiment - ~~is~~was concerned with enhancing the permeability of the rock mass with high pressure fluid injections. A *third and final phase*, (June – December 2017), the post-stimulation phase, ~~is~~was dedicated to characterize the rock mass in great detail after stimulation to quantify changes in permeability, fracture connectivity and heat exchanger properties.

Formatiert: Schriftart: Nicht Kursiv

### 3.2.1 Pre-Stimulation Phase – Rock mass characterization and Instrumentation

#### 3.2.1.1 Boreholes, rock mass characterization and geological model

The governing aspects for designing the instrumentation of the decameter-scale ISC experiment ~~are~~were 1) a detailed understanding of the geological settings in 3-dimensions (e.g., fracture and fault orientation and intersections, fracture density, etc.) 2) the in-situ state of stress, 3) the pre-stimulation hydraulic conditions, including the flow field, preferential fluid flow path ways and transmissivities, 4) the borehole sections used for stimulation, 5) the type of hydraulic injection (i.e., hydraulic shearing or hydraulic fracturing) and ~~4~~6) anticipated quantities and spatial distributions of strain, tilt and pressure within the rock volume during stimulation.

During the pre-stimulation phase a series of 15 cored boreholes with a length between 18 and 50 m and diameters between 86 and 146 mm ~~are~~were drilled within or about the experimental volume (Figure 3). Three boreholes ~~are~~were dedicated to stress measurements (SBH), two ~~for~~to the stimulation injections (INJ), four ~~for~~to geophysical characterization and monitoring (GEO), three ~~for~~to strain and temperature measurements (FBS) and another three ~~for~~to pore pressure, strain and temperature measurements (PRP). The boreholes ~~are~~were characterized in terms of geologic structures, hydraulic properties and inter-borehole connectivity ~~using various~~Various geological (i.e., core logging), geophysical (i.e., optical televiewer logs, resistivity logs ~~using a guard resistivity sonde~~, full-wave sonic logs, ground penetrating radar (GPR) surveys ~~with unshielded antennas~~ and active seismic measurements between the injection boreholes) and single-hole and cross-hole hydraulic methods (i.e., packer tests such as pressure-pulse, constant-rate and constant head injection tests, oscillating pumping tests, and tracer tests using various solutes, DNA-encoded nanoparticles, and heat~~-~~) were used. In addition to borehole-based characterization methods, the experimental rock volume was characterized using detailed tunnel maps, reflection GPR from the tunnel walls and active seismic data acquisition between the AU and VE tunnels (Figure 1b). The trajectories of the subsequent boreholes were chosen ~~based on the basis of~~ these preliminary geological and hydraulic data and simplified numerical HM-coupled models (i.e., using 3DEC, Itasca 2014) for stimulation scenarios that ~~provide~~provided an estimate of the deformation field and pore pressure propagation along geological structures.

The joint interpretation of ~~the above~~all geophysical ~~borehole logging, geological~~ and ~~imaging data, tunnel mapping, core logging and hydraulic test data were~~hydrogeological observations was used to constrain a 3D structural model of the experimental volume (Krietsch et al., 2017, Figure 4). The 3D model illustrates the intersection of the shear zones ~~that were targeted during~~

the ISC experiments within the experimental volume (Figure 4). S1 shear zones (numbered from north to south: S1.1 to S1.3) within the ISC test volume have similar orientations as the overall foliation in the rock mass. These shear zones are characterized by an increase in foliation intensity, and a few fractures with random distribution. The highest strains were localized in mm-thick mylonitic bands. Due to similar appearance and orientation, no distinction between S1 and S2 shear zones are made in the ISC volume. The experimental volume is crosscut in east-west direction by two major (up to 1 m thick) meta-basic dykes that are separated by 2 m. Within the ISC volume the S3 shear zones have the same orientation as the meta-basic dykes. Thus, each of the two shear zones (here referred to as S3.1 and S3.2) is localized along the major meta-basic dykes. Shearing of the meta-basic dykes appears to have been localized in fine ductile shear bands resulting in biotite-rich mylonitic shear bands (i.e. 1-2 cm thick). The dextral shearing of S3 led to a deformation of S1 faults around the meta-basic dykes (Figure 4). Multiple persistent, partly open fractures are located between and within the meta-basic dykes and within the host rock close to the fault. The volume between the two sheared dykes is characterized by a high brittle fracture density (i.e. more than 20 fractures per m) compared to the rest of the rock mass (0-3 fractures per meter; Krietsch et al., 2017). The orientations of these fractures are shown in Figure 4. The two metabasic dykes S3.1. and S3.2, and the brittle fracture zone between the shear zone is referred to as S3 fault zone.

Two major (up to 1 m thick) meta-basic dykes (S3.1 and S3.2) up to 1 m thick with a spacing of 2 m crosscut the volume in east-west direction. These metabasic dykes form the boundary of a zone with a high fracture density and partly open fractures, which together with the dykes define the S3 shear zone. The majority of brittle fractures within and outside the S3 shear zone are oriented parallel to the boundaries of the sheared metabasic dykes, which strike E-W in the test volume. Very few fractures penetrate into the dykes. Several quartz veins are present with strikes of NNE to E and widths ranging from millimetres up to 30 cm. However, the lateral extension of these quartz veins is limited to the meter range.

### 3.2.1.2 Rock mass instrumentation

In addition to a detailed characterization of the test volume for the design and interpretation of the in-situ experiment, a dense sensor network ~~is was~~ required to collect the necessary data at a sufficient spatial resolution that ~~are were~~ needed to address the previously mentioned ~~nine~~ research questions (i.e. ~~research question [1 to RQ1-9])~~. This includes: pore pressure monitoring [~~research questions 1, 2, 6~~], strain and tilt [~~research questions 1, 3, 4, 5, 6~~] and



micro-seismic monitoring [research questions 4, 5, 7, 8, 9]. A major aspect governing the detailed instrumentation. Instrumentation design is was also governed by the types of hydraulic injection treatment (i.e. treatments that were performed in the ISC experiment, i.e., hydraulic shearing (pressurization and reactivation of natural fractures and faults) and hydraulic fracturing or hydraulic shearing). For the ISC experiment both hydraulic fracturing (i.e., initiation and propagation of new fractures) and hydraulic shearing (i.e., pressurization of natural structures such as faults) are considered.

#### *Pore pressure, deformations and temperature*

To address questions related to hydro-mechanics (RQ1), pressure propagation (RQ2) and interaction between pre-existing and hydraulic fractures (RQ6), four pressure monitoring boreholes (three PRP boreholes and SBH15.004; Figure 3) are dedicated to the measurement of the pressure propagation [research questions 1, 2, 6] were instrumented at points where they cut relevant structures within the test volume during stimulation. These boreholes are completed with resin-grouted packer systems with fixed open intervals of few litres volume for pressure monitoring. The boreholes were drilled approximately normal to the strike of the main geological features. The intervals are chosen to capture the pore (S1 and S3 shear zones). They were completed with cement and resin-grouted packer systems with fixed open pressure monitoring intervals that record the pressure within fracture zones or fault zones. Pressure was also recorded in the INJ borehole that was not being injected in the test used for stimulation (Figure 3) by deploying with a straddle packer system similar to the one used for high pressure fluid injections. Pore pressure was monitored using a sampling rate of 20 Hz. The PRP boreholes were also equipped with pre-stressed distributed fibre optics (FO) cables for strain and temperature measurements. Strain recordings will give information on the HM response to pressurization across pre-existing fractures (e.g., research question 3 RQ1), and 9), as well as on help to detect propagation of new fractures during hydrofracturing experiment (e.g., research question 6 RQ6). Distributed temperature measurements are important for were used during pre- and post-stimulation thermal tracer tests.

Additional To address research questions related to rock mass deformations (RQ3-6), three boreholes (FBS16.001-3 in Figure 3) are dedicated to the measurement of rock mass deformation associated with hydraulic stimulation. The holes were equipped with both distributed and Fiber Bragg Grating (FBG) strain-sensing optical fibers that were grouted in place. One borehole (FBS16.001) is approximately normal to the strike of the main geological

features (i.e. ~~mean strike of~~ and intersects both the S3 and S1 fault zones, Figure 4) and thus intersects them. One Another borehole is parallel to the strike of the S3.1 fault and intersects the S1.1 fault (FBS16.002), and one is parallel to the S1.2 faults and intersects the S3 fault zone (FBS16.003). Axial strains developed ~~The FBG sensors record axial strain across borehole sections of the boreholes~~ that span potentially active fractures or the ‘intact’ rock mass ~~between them are measured with FBG sensors that have an operating range of 1000 to 2000  $\mu\epsilon$  and a resolution of 0.1  $\mu\epsilon$ . The objective to measure strain parallel to fault zones is to capture the strain field that is associated with fault shearing during stimulation. Strain sensors across structures allow quantifying the fracture dislocation.~~ Distributed strain-sensing optical fibers allow a dense spatial coverage and thus ~~increase the likelihood~~ are more likely to observe the propagation ~~direction~~ and opening of a hydraulic fracture. ~~A parallel distribution of untensioned Bragg Grating sensors is used to correct the strains for temperature. All FBG sensors are monitored with a 16 channel si255 Hyperion FBG interrogator (Miconoptics), which is able to record strain or relative temperature from more than 10 sensors per channel with sampling rates of up to 1000 Hz. By averaging up to 1000 samples the strain resolution can be improved to <0.1  $\mu\epsilon$ . All three FO boreholes are also equipped with a distributed pre-stressed fiber optics cable for strain and temperature monitoring that are recorded with a DiTest device from ominsense.~~

The borehole strain monitoring system ~~is~~ was complemented with an array of 3 biaxial tiltmeters installed on the margins of the test volume along the VE tunnel near the S3 fault zone (Figure 3). ~~They are~~ The tilt sensors were mounted in shallow holes drilled into the tunnel floor. ~~The tilt sensors are of type 711-2 from Applied Geomechnics, and have a resolution of 0.1  $\mu$ radians record horizontal tilt.~~ Together, the tilt measurements and the longitudinal strain in the FO boreholes ~~will~~ were capable to describe the deformation field around the stimulated rock volume and ~~allow~~ allowed constraining the characteristics of the stimulated fault ~~zone~~ zones (i.e., dimension, dislocation direction and magnitude, etc.), ~~which helps answering research questions 3, 4, 5, and 9.~~

## Micro seismicity

Microseismicity is monitored. Questions related to induced seismicity (RQ5, 7, 8) were tackled using a microseismic monitoring system, which consists of a sensor network with 14 piezo sensors (Type GMuG Ma-BIs 7-70) piezosensors affixed to the tunnel walls, and 8 sensors (type GMUG Ma-BIs 7-70) that were pressed pneumatically against the borehole wall in the geophysical monitoring boreholes (GEO16.001 – 4, Figure Figures 3 and 6). The distribution of sensors within and about the experimental volume ensures optimal azimuthal and vertical coverage around the stimulation points (5). The uncalibrated piezo sensors are piezosensors were complemented with calibrated accelerometers (Type Wileoxon 736Tas done by Kwiatak et al., 2011) at five locations on the tunnel surface to enable the calculation of absolute magnitudes. The piezo sensors are sensitive to strain signals in the range of 1-100 kHz, while the accelerometers are sensitive from 50 Hz to 40 kHz. Signals from all sensors were recorded continuously on a 32-channel acquisition system (provided by Gesellschaft für Materialprüfung und Geophysik, GMuG) at a sampling rate of 1 MHz. An A real-time event detection, first arrival determination and location algorithm with automatic picking of first arrivals allows real time computation of gave provisional event hypocentres. More detailed processing of the complete data is performed after the experiment (Gischig et al., 2017). Recorded induced seismicity is the basis to answer research question 5, 7 and 8.

The sensor network is was also used to recorded periodic active seismic experiments. Highly reproducible sources (i.e., piezoelectric pulse sources in boreholes and hammers installed at the tunnel walls with pre-defined constant fall height, Figure 6) are 5) were triggered roughly every 10 minutes during the stimulation experiments with the goal of recording systematic changes in the waveform characteristics that allow inferring changes of seismic velocity, attenuation and scattering properties. Such measurements can give additional constraints on 3D pressure propagation and deformation characteristics (research question 1 – 4 and RQ1-4, 9).

## 3.3 Stimulation Phase

As both hydroshearing and hydrofracturing are part of above research questions, the The stimulation experiments consist of were performed in two parts: 1) experiment sequences: 1) In February 2017, six hydraulic shearing experiments were performed including high-pressure water injection into existing faults or fracture zones within the test volume so that the so as to reduce effective normal stress on the structures is reduced and hydraulic trigger shearing is triggered, and 2) In May 2017, six hydraulic fracturing experiments were conducted with high

pressure injection into fracture-free borehole intervals so as to initiate and propagate hydraulic fractures.

Two 146-mm diameter, downwardly-inclined boreholes (INJ 1 and INJ 2 in Figure 3) ~~are~~were dedicated for the ~~hydraulic shearing and hydraulic fracturing stimulation~~ injections from packer-isolated intervals. For the stimulation operations, water or gel ~~is~~was injected into a 1-2 m interval in one borehole, and the second borehole ~~is~~was used to additionally monitor the fluid pressure response, ~~together with other dedicated pressure monitoring boreholes.~~ The maximum injected volume for the stimulation at each interval ~~is~~was limited to about 1000 liters, ~~in order.~~ This value was determined as part of a pre-experiment hazard and risk study (Gischig et al., 2016) and was found to minimize the acceptable regarding the estimated likelihood of inducing seismic events that could be felt in the tunnels, as well as avoid the disturbance to ongoing experiments elsewhere in the GTS. We used standardized injection protocols for HS and HF (i.e., we did not test different injection strategies) so that the variability in the rock mass response arises from differences of local hydromechanical conditions as well as geological settings, and not from different injection strategies.

### 3.3.1 Hydroshearing ~~experiment~~experiments

The stimulation injections ~~target~~targeted natural fracture zones in the rock volume ~~whose transmissivities ranges from 1e-87 to 1e-1110 m<sup>2</sup>/s.~~ Each interval stimulation ~~consists~~consisted of ~~three~~four cycles (Figure ~~7~~6). The objective of the first cycle ~~is~~was to measure initial transmissivity and jacking pressure, and break down the interval. Initially (Cycle ~~1~~1), pressure ~~needs to be~~was increased in small steps until breakdown ~~occurs~~occurred, as evidenced by a disproportionate increase in flow rate. This first ~~sub-cycle~~ allows to quantify~~allowed quantifying~~ the initial injectivity. After venting, the test ~~needs to be~~was repeated with refined pressure steps (Cycle ~~1~~2) in a narrow range to identify the jacking pressure. After Cycle ~~1~~2 the interval ~~is~~was shut-in to capture the pressure decline curve before the interval ~~is~~was vented. The purpose of the ~~second~~third cycle ~~is~~was to increase the extent of the stimulation away from the injection interval. For this purpose, a step-rate injection test with four or more steps ~~is~~was utilized ~~with a maximum rate of 37 l/min.~~ The interval ~~is~~was then shut-in and the pressure decline ~~is~~was monitored for 40 minutes before initiating venting for 30 minutes. The purpose of the ~~third~~fourth cycle ~~is~~was to determine post-stimulation interval transmissivity and jacking pressure for comparison with pre-stimulation values. Thus, a step-pressure test ~~is~~was conducted initially taking small pressure steps to define the low-pressure Darcy trend and the deviation

from it ~~that occurs at~~ defining the jacking pressure. Following this cycle, the interval ~~is~~ was shut-in for 10 minutes before venting. An important aspect for the quantification of irreversible changes in the reservoir ~~is~~ was to run acoustic televiewer logs across each interval before and after the stimulation to attempt to resolve any dislocation that may occur across the fractures in the interval.

### 3.3.2 Hydraulic fracturing experiment

The protocol for hydraulic fracturing tests in borehole intervals without natural fractures ~~are~~ is shown in Figure 8. ~~Again, each~~ 7. Each interval stimulation ~~consists~~ consisted of three cycles. First, the packed interval ~~is~~ was tested with a pulse for integrity. ~~The measured transmissivity in intact rock ranges from  $1\text{e-}13$  to  $1\text{e-}14$  m<sup>2</sup>/s.~~ The objective of the first cycle ~~is~~ was to break down the formation (i.e., to initiate a hydraulic fracture) using small flow rates (i.e., around 5 l/min injections for 60 s). The second cycle ~~aims~~ aimed to propagate the hydraulic fracture away from the ~~well bore~~ wellbore and connect to the pre-existing fracture network using progressively increasing flow rates (up to 100 l/min). ~~A shut-in and venting period follows~~ followed. Finally, ~~The purpose of the third cycle~~ ~~is~~ was to quantify the final injectivity and jacking pressure using a pressure step ~~injections~~ injection similar to the pressure step injection considered for cycle 34 in the fault slip experiments. Both pure water and a gel (i.e., a Xanthan-water-salt-mixture with 0.025 weight percent of Xanthan and 0.1 weight percent of salt with a viscosity between 35 and 40 cPs) ~~are~~ were used for fracture propagation. ~~If gel is~~ was used, cycle 2 is extended with a flushing cycle (with water) after fracture propagation. The two injection fluids ~~allow~~ allowed investigating two different propagation regimes (i.e., toughness-dominated and viscous-dominated). ~~A specific amount of salt was added to each injection fluid as a tracer, to investigate flow paths and dilution effects.~~ Further, a cyclic injection sequence ~~is~~ was included ~~into~~ in the fracture propagation cycle to test ~~it~~ as an alternative injection protocol as proposed by Zang et al. (2013). ~~They propose~~ proposed that using cyclic injection the same efficiency in fracture propagation can be reached, while the associated micro-seismic event release is limited and fracture branching is enhanced.

### 3.4 Post-Stimulation Phase

~~The purpose of this~~ In the last experiment phase ~~is to determine~~, the changes to the hydrology and rock mass properties that occurred ~~as a result~~ because of each of the two stimulations phases (i.e., the hydraulic shearing and hydraulic fracturing phases) ~~.)~~ were investigated. Accordingly,

after each phase, a characterization program was performed. The hydraulic properties of the rock mass were determined using single-hole and cross-hole hydraulic methods similar to pre-stimulation the characterization phase. ~~Selected stimulation intervals were isolated with packers and then subjected to a variety of tests including pressure pulse, constant rate and constant head injection tests, oscillating pumping tests, and tracer tests using solute dyes, DNA-tagged nanoparticles and heat.~~ In addition, single hole, cross-hole, and cross-tunnel active seismic and GPR measurements were conducted. ~~Repeat geophysical borehole logs were run in both injection boreholes, including focused resistivity, and full-wave sonic.~~

#### 4 Summary and Conclusion

The review of scientific research results showed that carefully analyzed data from large-scale experiments (i.e., EGS projects) and laboratory scale experiments provide a fundamental understanding of processes that underpin permeability creation and induced seismicity in EGS. The results from large-scale experiments suffer from accessibility and resolution, which does not permit to resolve the details of seismo-hydro-mechanical coupled processes associated with the stimulation process. Laboratory scale experiment provide a fundamentally improved understanding of these processes but suffer from scalability and test conditions that may lead to over-simplistic fracture flow and/or hydraulic fracture propagation behavior that is not representative for a heterogeneous reservoir. Intermediate-scale experiments can serve to bridge the gap between the laboratory and the large scale and may enable upscaling of results gained from small scale experiments. However, only few intermediate-scale hydro-shearing and hydro-fracturing experiments have recently been performed in a densely instrumented rock mass and no such measurements have been performed on faults in crystalline basement rocks.

We have provided here an overview of the intermediate scale hydroshearing and hydrofracturing experiment (i.e., ISC experiment) ~~is being~~that was executed in 2017 in the naturally fractured and faulted crystalline rock mass at the Grimsel Test Site (Switzerland). It ~~is was~~ designed to fill some of the key research gaps and thus contribute to a better understanding of seismo-hydro-mechanical processes associated with the creation of Enhanced Geothermal Systems. As this contribution is meant to only provide a literature review and an overview of our ISC experiment at the Grimsel Test Site, several other publications will provide more detailed descriptions and analyses of this intermediate-scale hydroshearing and hydrofracturing experiment.

## 5 Acknowledgment

The ISC is a project of the Deep Underground Laboratory at ETH Zurich, established by the Swiss Competence Center for Energy Research - Supply of Electricity (SCCER-SoE) with the support of the Swiss Commission for Technology and Innovation (CTI). Funding for the ISC project was provided by the ETH Foundation with grants from Shell and EWZ and by the Swiss Federal Office of Energy through a P&D grant. Hannes Krietsch is supported by SNF grant 200021\_169178. The Grimsel Test Site is operated by Nagra, the National Cooperative for the Disposal of Radioactive Waste. We are indebted to Nagra for hosting the ISC experiment in their GTS facility and to the Nagra technical staff for onsite support. We also thank two anonymous reviewers for their valuable input.

## 56 References

- Achtziger-Zupančič P., Loew S. and Mariéthoz G. (2017). A new global database to improve predictions of permeability distribution in crystalline rocks at site scale. *Journal of Geophysical Research. Solid Earth*, 122 (5): 3513-3539, Washington, DC: American Geophysical Union.
- Adams, B.M., T.H. Kuehn, J.M. Bielicki, J.B. Randolph, and M.O. Saar (2014). On the importance of the thermosiphon effect in CPG (CO<sub>2</sub> Plume Geothermal) power systems, *Energy*, DOI: 10.1016/j.energy.2014.03.032, 69:409-418.
- Adams, B.M., T.H. Kuehn, J.M. Bielicki, J.B. Randolph, M.O. Saar (2015). A Comparison of Electric Power Output of CO<sub>2</sub> Plume Geothermal (CPG) and Brine Geothermal Systems

1012 for Varying Reservoir Conditions, Applied Energy, DOI:  
 1013 10.1016/j.apenergy.2014.11.043, 140:365–377.

1014 Ake J, Mahrer K, O’Connell D, Block L. (2005). Deep-Injection and Closely Monitored  
 1015 Induced Seismicity at Paradox Valley, Colorado. Bulletin of the Seismological Society of  
 1016 America, 95(2), 664–683. doi:10.1785/0120040072

1017 Amitrano, D., (2012). Variability in the power-law distributions of rupture events, Eur. Phys.  
 1018 J. Spec. Top., 205, 199–215.

1019 Amitrano, D., and J. Schmittbuhl (2002), Fracture roughness and gouge distribution of a granite  
 1020 shear band, *J. Geophys. Res.*, 107(B12), 2375 doi:10.1029/2002JB001761.

1021 Asanuma H, Soma N, Kaieda H, Kumano Y, Izumi T, Tezuka K, et al. (2005). Microseismic  
 1022 monitoring of hydraulic stimulation at the Australian HDR project in Cooper Basin. In  
 1023 Proceedings World Geothermal Congress (pp. 24–29).

1024 Bachmann, C., S. Wiemer, B. P. Goertz-Allmann, J. Woessner (2012). Influence of pore  
 1025 pressure on the size distribution of induced earthquakes, Geophysical Research Letters, 38,  
 1026 L09308.

1027 Bachmann, C., S. Wiemer, J. Woessner, S. Hainzl (2011). Statistical analysis of the induced  
 1028 Basel 2006 earthquake sequence: Introducing a probability-based monitoring approach for  
 1029 Enhanced Geothermal Systems, Geophys. J. Int.

1030 Baisch, S., Vörös, R., Rothert, E., Stang, H., Jung, R. Schellschmidt, R., (2010). A numerical  
 1031 model for fluid injection induced seismicity at Soutz-sous-Forêt, Int. J. Rock Mech. Min. Sci.,  
 1032 47, 405–413. Baisch, S., Harjes, H.P. (2003). A model for fluid-injection-induced seismicity at  
 1033 the KTB, Germany. Geophysical Journal International 152, 160–170.

1034 Baisch, S., R. Vörös, R. Weidler, D. Wyborn (2009). Investigation of fault mechanisms during  
 1035 geothermal reservoir stimulation experiments in the Cooper Basin (Australia), Bull. Seismol.  
 1036 Soc. Am. 99, no. 1, 148–158.

1037 Baisch, S., R. Weidler, R. Vörös, D. Wyborn, L. DeGraaf (2006). Induced seismicity during  
 1038 the stimulation of a geothermal HFR reservoir in the Cooper Basin (Australia), Bull. Seismol.  
 1039 Soc. Am. 96, no. 6, 2242–2256.

1040 Baisch, S., Rothert, E., Stang, H., Vörös, R., Koch, Ch., McMahon, A. (2015). Continued  
 1041 Geothermal Reservoir Stimulation Experiments in the Cooper Basin (Australia). Bulletin of the  
 1042 Seismological Society of America, Vol. 105, No. 1, pp. 198–209

Formatiert: Deutsch (Schweiz)

Formatiert: Deutsch (Schweiz)



1043 Bandis S., A.C. Lumsden, N. R. Barton (1983). Fundamentals of rock joint deformation.  
 1044 International Journal of Rock Mechanics Mining Sciences & Geomech Abstr., 20, 6: 249–268.

1045 Bao X., Eaton D. W. (2016). Fault activation by hydraulic fracturing in western Canada.  
 1046 Science 10.1126/science.aag2583

1047 Baria, R., and A. S. P. Green (1986), Seismicity induced during a viscous stimulation at the  
 1048 Camborne School of Mines Hot Dry Rock Geothermal Energy project in Cornwall, England,  
 1049 paper presented at 8th Int. Acoustic Emission Symp., Japanese Soc. of NDI, Tokyo, Japan,  
 1050 October.

1051 Barton C.A., M. D. Zoback, D. Moos (1995). Fluid-flow along potentially active faults in  
 1052 crystalline rock. *Geology*, 23, 8: 683–686

1053 Barton N., S. Bandis, K. Bakhtar (1985). Strength, deformation and conductivity coupling of  
 1054 rock joints. *Int. J. Rock Mech. Min. Sic. & Geomech. Abstr.* 22, 121-140.

1055 Barton, C.A., S. Hickman, R. Morin, M.D. Zoback, R. Benoit (1998). Reservoir-scale fracture  
 1056 permeability in the Dixie Valley, Nevada, Geothermal Field, paper 47371 presented at  
 1057 SPE/ISRM Eurock '98, Soc. of Pet. Eng., Trondheim, Norway.

1058 Barton, N.A., Choubey, V., 1977. The shear strength of rock joints in theory and practice. *Rock*  
 1059 *Mechanics* 10, 1-34.

1060 Batchelor, A. S., R. Baria, and K. Hearn (1983), Monitoring the effects of hydraulic stimulation  
 1061 by microseismic event location: a case study, in *58th Ann. Tech. Conf. and Exhibition of SPE*,  
 1062 edited, Soc. Petrol. Eng., San Francisco, California.

1063 Baujard, C., Bruel, D., (2006). Numerical study of the impact of fluid density on the pressure  
 1064 distribution and stimulated volume in the Soultz HDR reservoir, *Geothermics*, 35, 607–  
 1065 621. Bennour Z, Ishida T, Nagaya Y, Chen Y, Nara Y, Chen Q, Sekine K, Nagano Y (2015)  
 1066 Crack extension in hydraulic fracturing of shale cores using viscous oil, water, and liquid  
 1067 carbon dioxide. *Rock Mech Rock Eng* 48(4):1463–1473 Biot, M.A. (1941). General theory of  
 1068 three dimensional consolidation. *Journal of Applied Physics*. 12: 155–164.

1069 Blake, K., and N. Davatzes (2011), Crustal stress heterogeneity in the vicinity of COCO  
 1070 geothermal field, CA., paper presented at 36th Workshop on Geothermal Reservoir  
 1071 Engineering, Stanford University, Stanford University, Jan31-Feb2.

1072 Block L., Wood C., Yeck W., King V. (2015). Induced seismicity constraints on subsurface  
 1073 geological structure, Paradox Valley, Colorado. *Geophysical Journal International*, 200(2),  
 1074 1170–1193. doi:10.1093/gji/ggu459

1075 Bommer, J.J., Oates, S., Cepeda, J.M., Lindholm, C., Bird, J., Torres, R., Marroquín, G., Rivas,  
1076 J., (2006). Control of hazard due to seismicity induced by a hot fractured rock geothermal  
1077 project, *Eng. Geol.*, 83, 287–306.

1078 Boroumand N, Eaton D. (2012). Comparing Energy Calculations - Hydraulic Fracturing and  
1079 Microseismic Monitoring. Presented at the Geoconvention 2012 - 74th Mtg., EAGE,  
1080 Copenhagen, C042.

1081 Breede, K., Dzebisashvili, K., Liu, X., and Falcone, G. (2013). A systematic review of enhanced  
1082 (or engineered) geothermal systems: past, present and future. *Geothermal Energy*, 1(1):1.

1083 Brown, D.W., (2000). A hot dry rock geothermal energy concept utilizing supercritical CO<sub>2</sub>  
1084 instead of water. In: *Proceedings of the Twenty-Fifth Workshop on Geothermal Reservoir*  
1085 *Engineering*, Stanford, CA. Stanford University.

1086 Brown, D. W., Duchane, D. V., Heiken, G., and Hriscu, V. T. (2012). *Mining the Earth's heat:*  
1087 *hot dry rock geothermal energy*. Springer Science & Business Media.

1088 Bruno M, Nakagawa F. (1991). Pore pressure influence on tensile fracture propagation in  
1089 sedimentary rock. *International Journal of Rock Mechanics and Mining Sciences &*  
1090 *Geomechanics Abstracts*, 28(4), 261–273. doi:10.1016/0148-9062(91)90593-b

1091 Bunger A, Detournay E, Garagash D, Peirce A, others. (2007). Numerical simulation of  
1092 hydraulic fracturing in the viscosity dominated regime. In *SPE Hydraulic Fracturing*  
1093 *Technology Conference*. Society of Petroleum Engineers.

1094 Bunger AP, Jeffrey RG, Kear J, Zhang X. (2011). Experimental Investigation of the Interaction  
1095 among Closely Spaced Hydraulic Fractures. In *45th US Rock Mechanics / Geomechanics*  
1096 *Symposium* (pp. 11–318+). San Francisco.

1097 Buscheck, T.A., J.M. Bielicki, T.A. Edmunds, Y. Hao, Y. Sun, J.B. Randolph, and M.O. Saar  
1098 (2016). Multifluid geo-energy systems: Using geologic CO<sub>2</sub> storage for geothermal energy  
1099 production and grid-scale energy storage in sedimentary basins, *Geosphere*, DOI:  
1100 10.1130/GES01207.1, 12(3):678-696.

1101 Byerlee, J. (1978). Friction of rocks. *Pure and applied geophysics*, 116(4-5):615-626.

1102 Caine, J. S., Evans, J. P., and Forster, C. B. (1996). Fault zone architecture and permeability  
1103 structure. *Geology*, 24(11):1025-1028.

1104 [Calo et al. \(2011\) Valentin](#)

1105 [Calò, M., Dorbath, C., Cornet, F. H., & Cuenot, N. \(2011\). Large-scale aseismic motion](#)  
1106 [identified through 4-DP-wave tomography. \*Geophysical Journal International\*, 186\(3\), 1295-](#)  
1107 [1314.](#)

1108 [Candela, T., Brodsky, E. E., Marone, C., & Elsworth, D. \(2014\). Laboratory evidence for](#)  
1109 [particle mobilization as a mechanism for permeability enhancement via dynamic stressing.](#)  
1110 [Earth and Planetary Science Letters, 392, 279-291.](#)

1111 Catalli, F., M.-A. Meier, S. Wiemer (2013). Coulomb stress changes at the Basel geothermal  
1112 site: can the Coulomb model explain induced seismicity in an EGS? *Geophys. Res. Lett.*, 40.

1113 Chacón E, Barrera V, Jeffrey R, van As A. (2004). Hydraulic fracturing used to precondition  
1114 ore and reduce fragment size for block caving. Presented at the MassMin 2004 Santiago Chile.

1115 Chen, Z., S. P. Narayan, Z. Yang, and S. S. Rahman (2000), An experimental investigation of  
1116 hydraulic behaviour of fractures and joints in granitic rock, *Int. J. Rock Mech. & Min. Sci.*, 37,  
1117 1061-1071.

1118 Chitrala, Y., C. Moreno, C. H. Sondergeld, and C. S. Rai (2010), Microseismic mapping of  
1119 laboratory induced hydraulic fractures in anisotropic reservoirs, paper presented at Tight Gas  
1120 Completions Conference, Society of Petroleum Engineers.

1121 Cornet F. H., Helm J., Poitrenaud H., Etchecopar A. (1997). Seismic and Aseismic Slips  
1122 Induced by Large-scale Fluid Injections. *Pure appl. geophys.* 150 (1997) 563–583

1123 Cornet F.H., Li L., Hulin J.-P., Ippolito I., Kurowski P. (2003). The hydromechanical  
1124 behaviour of a fracture: an in situ experimental case study. *International Journal of Rock*  
1125 *Mechanics & Mining Sciences* 40 (2003) 1257–1270

1126 Cornet, F. H., and J. Desroches (1989), The problem of channeling in Hot Dry Rock reservoirs,  
1127 paper presented at Camborne School of Mines International Hot Dry Rock Conference,  
1128 Robertson Scientific Publishers, Llandudno, UK, Cornwall, UK.

1129 Cornet, F. H., and O. Scotti (1993), Analysis of induced seismicity for fault zone identification,  
1130 *Int. J. Rock Mech. Min. Sci. & Geomech. Abst.*, 30(7), 789-795.

1131 Cornet, F. H., and R. H. Jones (1994), Field evidence on the orientation of forced water flow  
1132 with respect to the regional principal stress directions, paper presented at 1st North American  
1133 Rock Mechanics Symposium, Balkema, Austin, Texas.

1134 Cornet, F.H. (2012). The relationship between seismic and aseismic motions induced by forced  
1135 fluid injections. *Hydrogeology Journal* 20: 1463–1466.

1136 Das I, Zoback MD. (2011). Long-period, long-duration seismic events during hydraulic fracture  
 1137 stimulation of a shale gas reservoir. *The Leading Edge*, 30(7), 778–786. doi:10.1190/1.3609093

1138 Davies, R., Foulger, G., Bindley, A., Styles, P. (2013). Induced seismicity and hydraulic  
 1139 fracturing for the recovery of hydrocarbons, *Marine and Petroleum Geology*, 45, 171-185.

1140 Deichmann, N., J. Ernst (2009). Earthquake focal mechanisms of the induced seismicity in 2006  
 1141 and 2007 below Basel (Switzerland), *Swiss J Geosci*, 102(3), 457-466.

1142 Deichmann, N., Kraft, T., Evans, K.F, (2014). Identification of faults activated during the  
 1143 stimulation of the Basel geothermal project from cluster analysis and focal mechanisms of the  
 1144 larger magnitude events. *Geothermics*, 52 (2014) 84–97.

1145 Derode B., F. Cappa, Y. Guglielmi, J. Rutqvist (2013). Coupled seismo-hydromechanical  
 1146 monitoring of inelastic effects on injection-induced fracture permeability. *International Journal*  
 1147 *of Rock Mechanics & Mining Sciences* 61: 266–274

1148 Detournay, E. (2016). Mechanics of Hydraulic Fractures. In Davis, SH and Moin, P, (eds),  
 1149 *Annual Review of Fluid Mechanics*, vol 48, p. 311-339.

1150 Dusseault MB, McLennan J, Shu J. (2011). Massive multi-stage hydraulic fracturing for oil and  
 1151 gas recovery from low mobility reservoirs in China. *Petroleum Drilling Techniques*, 39(3), 6–  
 1152 16.

1153 Edwards, B., Kraft, T., Cauzzi, C., Kaestli, P., and Wiemer, S. (2015). Seismic monitoring and  
 1154 analysis of deep geothermal projects in St Gallen and Basel, Switzerland. *Geophysical Journal*  
 1155 *International*, 201(2):1020-1037.

1156 Ellsworth, W.L. (2013). Injection-induced earthquakes. *Science*, 12, 341, 6142

1157 [Elsworth, D., Fang, Y., Gan, Q., Im, K. J., Ishibashi, T., & Guglielmi, Y. \(2016, April\). Induced](#)  
 1158 [seismicity in the development of EGS—benefits and drawbacks. In \*Rock Dynamics: From\*](#)  
 1159 [Research to Engineering: Proceedings of the 2nd International Conference on Rock Dynamics](#)  
 1160 [and Applications \(p. 13\). CRC Press.](#)

1161 Emmermann R, Lauterjung J. (1997). The German Continental Deep Drilling Program KTB:  
 1162 Overview and major results. *J. Geophys. Res.*, 102(B8), 18179–18201. doi:10.1029/96jb03945

1163 Esaki T., H. Hojo, T. Kimura, N. Kameda, E. (1991). Shear-Flow Coupling Test on Rock joints.  
 1164 *Proceedings – Seventh International Congress on Rock Mechanics*, Vol 1: Rock Mechanics and  
 1165 Environmental Protection.

1166 Esaki, T., Du, S., Mitani, Y., Ikusada, K., Jing, L., (1999). Development of a shear-flow test  
 1167 apparatus and determination of coupled properties for a single rock joint, *Int. J. Rock Mech.*  
 1168 *Min. Sci.*, 36, 641–650.

1169 Evans K. F., F. H. Cornet, T. Hashida, K. Hayashi, T. Ito, K. Matsuki, T. Wallroth (1999).  
 1170 Stress and rock mechanics issues of relevance to HDR/HWR engineered geothermal systems:  
 1171 review of developments during the past 15 years. *Geothermics* 28, 455-474

1172 Evans K. F., H. Moriya, H. Niitsuma, R.H. Jones, W.S. Phillips, A. Genter, J. Sausse, R. Jung,  
 1173 R. Baria (2005a). Microseismicity and permeability enhancement of hydrogeologic structures  
 1174 during massive fluid injections into granite at 3 km depth at the Soultz HDR site, *Geophys. J.*  
 1175 *Int.*, 160, 388–412.

1176 Evans K.F. (2005). Permeability creation and damage due to massive fluid injections into  
 1177 granite at 3.5 km at Soultz: 2. Critical stress and fracture strength, *J. geophys. Res.*, 110.

1178 Evans K.F., A. Genter, J. Sausse (2005b). Permeability creation and damage due to massive  
 1179 fluid injections into granite at 3.5 km at Soultz: 1. Borehole observations. *J. geophys. Res.*, 110,  
 1180 B04203.

1181 Evans K.F., F. Wyatt (1984). Water table effects on the measurement of earth strain.  
 1182 *Tectonophysics*, 108: 323-337

1183 Evans K.F., T. Kohl, L. Rybach, R.J. Hopkirk (1992). The effect of fracture normal compliance  
 1184 on the long-term circulation behaviour of a hot dry rock reservoir: A parameter study using the  
 1185 new fully coupled code fracture. *Geothermal Resources Council Transactions*, Vol. 16, 449-  
 1186 456, San Diego, CA

1187 Evans, J.P., Forster, C.B., Goddard, J.V. (1997). Permeability of fault-related rocks, and  
 1188 implications for hydraulic structure of fault zones. *J. Struct. Geol.* 19, 1393–1404.

1189 Evans, K. F. (1983), Some examples and implications of observed elastic deformations  
 1190 associated with the growth of hydraulic fractures in the Earth, paper presented at Workshop on  
 1191 Hydraulic Fracturing Stress Measurements, National Academy Press, Monterey, California.

1192 Evans, K. F. (1998). Does significant aseismic slip occur on fractures in HDR systems under  
 1193 stimulation conditions? *Proceedings*, 4th Int. HDR Forum Strasbourg, September 28-30th.

1194 Evans, K. F., and P. Meier (1995), Hydro-jacking and hydrofracturing tests in a fissile schist in  
 1195 south-west Switzerland: In-situ stress characterisation in difficult rock, paper presented at 2nd  
 1196 Int. Conf. on the Mechanics of Jointed and Faulted Rock, Balkema, Vienna, 10-14 April.

1197 Evans, K. F., and S. Sikaneta (2013), Characterisation of natural fractures and stress in the Basel  
 1198 reservoir from wellbore observations (Module 1), in *GEOTHERM: Geothermal Reservoir*  
 1199 *Processes: Research towards the creation and sustainable use of Enhanced Geothermal*  
 1200 *Systems*, edited by K. F. Evans, pp. 9-18, Swiss Federal Office of Energy Publication No  
 1201 290900, Bern.

1202 Evans, K. F., Zappone, A., Kraft, T., Deichmann, N., and Moia, F. (2012). A survey of the  
 1203 induced seismic responses to uid injection in geothermal and co 2 reservoirs in Europe.  
 1204 *Geothermics*, 41: 30-54.

1205 Evans, K., Holzhausen, G. (1983). On the development of shallow hydraulic fractures as viewed  
 1206 through the surface deformation field: Part 2-case histories. *Journal of Petroleum Technology*,  
 1207 35(02):411-420.

1208 Evans, K., Wieland, U., Wiemer, S., Giardini D. (2014). Deep Geothermal Energy R&D  
 1209 Roadmap for Switzerland, 2014.

1210 Evans, K. F. (2014), Reservoir Creation, in *Energy from the Earth - Deep Geothermal as a*  
 1211 *Resource for the Future?*, edited by S. Hirschberg, S. Wiemer and P. Burgherr, pp. 82-118,  
 1212 Zentrum für Technologiefolgen-Abschätzung, Bern.

1213 Eyre, T. S., and M. van der Baan (2015), Overview of moment-tensor inversion of microseismic  
 1214 events, *The Leading Edge*, August, 882-888 doi: 10.1190/tle34080882.1.

1215 [Fang, Y., Elsworth, D., Wang, C., Ishibashi, T., & Fitts, J. P. \(2017\). Frictional stability-](#)  
 1216 [permeability relationships for fractures in shales. \*Journal of Geophysical Research: Solid Earth\*.](#)  
 1217 [122\(3\), 1760-1776.](#)

1218 [Fang, Y., Elsworth, D., & Cladouhos, T. T. \(2018\). Reservoir permeability mapping using](#)  
 1219 [microearthquake data. \*Geothermics\*, 72, 83-100.](#)

1220 Faulkner D., Jackson, C., Lunn, R., Schlische, R., Shipton, Z., Wibberley, C., Withjack, M.,  
 1221 (2010). A review of recent developments concerning the structure, mechanics and fluid flow  
 1222 properties of fault zones. *J. Struct. Geol.* 32, 1557–1575.

1223 Faulkner D.R., and E.H. Rutter (2008). Can the maintenance of overpressured fluids in large  
 1224 strike-slip fault zones explain their apparent weakness? *Geology* 29, no. 6: 503–506.

1225 Gale, J. E. (1975). A numerical, field and laboratory study of flow in rocks with deformable  
 1226 fractures. Ph.D. dissertation, Berkeley, University of California, 255 p.

1227 Gale, J. E. (1993). Fracture properties from laboratory and large scale field tests: evidence of  
 1228 scale effects. Scale Effects in Rock Masses. Proc. 2nd Int. Workshop on Scale Effects in Rock  
 1229 Masses (Edited by Pinto da Cunha A.), Lisbon, pp. 341-352. Balkema, Rotterdam.

1230 Garagash, D.I., L.N., Germanovich (2012). Nucleation and arrest of dynamic slip on a  
 1231 pressurized fault, J. Geophys. Res., 117, B10310.

1232 Garapati, N., J.B. Randolph, and M.O. Saar (2015). Brine displacement by CO<sub>2</sub>, energy  
 1233 extraction rates, and lifespan of a CO<sub>2</sub>-limited CO<sub>2</sub> Plume Geothermal (CPG) system with a  
 1234 horizontal production well, Geothermics, DOI: 10.1016/j.geothermics.2015.02.005, 55:182–  
 1235 194.

1236 [Garcia, J., Walters, M., Beall, J., Hartline, C., Pingol, A., Pistone, S., & Wright, M. \(2012, January\). Overview of the northwest Geysers EGS demonstration project. In Proceedings, Thirty-Seventh Workshop on Geothermal Reservoir Engineering Stanford University.](#)

1239 Genter A. , Goerke X., Graff J.-J., Cuenot N., Krall G., Schindler M., Ravier G. (2010). Current  
 1240 Status of the EGS Soultz Geothermal Project (France). Proceedings World Geothermal  
 1241 Congress 2010, Bali, Indonesia, 25-29 April 2010

1242 Gentier, S., D. Hopkins, and J. Riss (2000). Role of fracture geometry in the evolution of flow  
 1243 paths under stress, in Dynamics of Fluids in Fractured Rock, Geophys. Monogr. Ser., vol. 122,  
 1244 edited by B. Faybishenko, P. A. Witherspoon, and S. M. Benson, pp. 169 – 184, AGU,  
 1245 Washington, D. C.

1246 Giardini, D. (2009). Geothermal quake risks must be faced, Nature, 462 (7275), 848-849.

1247 Gischig, V., G. Preisig (2015), Hydro-fracturing versus hydro-shearing: a critical assessment  
 1248 of two distinct reservoir stimulation mechanisms, paper presented at International Congress of  
 1249 Rock Mechanics, ISRM 2015, Montréal, Canada.

1250 Gischig, V.S., J. Doetsch, H. Maurer, H. Krietsch, F. Amann, K.F. Evans, M. Nejati, M.R.  
 1251 Jalali, A. Obermann, B. Valley, S. Wiemer, and D. Giardini (2017). On the link between stress  
 1252 field and small-scale hydraulic fracture growth in anisotropic rock derived from micro-  
 1253 seismicity. Submitted to Solid Earth.

1254 [Gischig, V., Jalali, M., Amann, F., Krietsch, H., Klepikova, M., Esposito, S., Broccardo, M., Obermann, A., Mignan, A., Doetsch, J., Madonna, C. \(2016\). Impact of the ISC Experiment at the Grimsel Test Site-Assessment of Potential Seismic Hazard and Disturbances to Nearby Experiments and KWO Infrastructure. ETH Zurich, <https://doi.org/10.3929/ethz-b-000189973>.](#)

1258 [Gischig, V. S. \(2015\). Rupture propagation behavior and the largest possible earthquake](#)  
1259 [induced by fluid injection into deep reservoirs. Geophysical Research Letters, 42\(18\):7420-](#)  
1260 [7428.](#)

1261 [Gischig, V. S., Wiemer, S., Alcolea, A. R. \(2014\). Balancing reservoir creation and seismic](#)  
1262 [hazard in enhanced geothermal systems. Geophysical Journal International. doi:](#)  
1263 [10.1093/gji/ggu221](#)

1264 Gischig, V.S., Wiemer, S. (2013). A stochastic model for induced seismicity based on non-  
1265 linear pressure diffusion and irreversible permeability enhancement, *Geophys. J. Int.*, 194(2),  
1266 1229–1249.

1267 Goebel, T. H. W., T. W. Becker, D. Schorlemmer, S. Stanchits, C. Sammis, E. Rybacki, G.  
1268 Dresen (2012). Identifying fault heterogeneity through mapping spatial anomalies in acoustic  
1269 emission statistics, *J. Geophys. Res.*, 117, B03310.

1270 Goertz-Allmann, B.P., Wiemer, S. (2013). Geomechanical modeling of induced seismicity  
1271 source parameters and implications for seismic hazard assessment, *Geophysics*, 78(1), KS25–  
1272 KS39.

1273 Goertz-Allmann, B.P., Goertz, A., Wiemer, S. (2011). Stress drop variations of induced  
1274 earthquakes at the Basel geothermal site, *Geophys. Res. Lett.* 38(9), L09308.

1275 Goodman R. E. (1974). The mechanical properties of joints. *Proceedings of the 3rd Int. Congr.*  
1276 *International Society of Rock Mechanics*, Denver, Colorado. National Academy of Sciences,  
1277 Washington, DC, I, 127–140.

1278 Guglielmi Y., F. Cappa, H. Lancon, J. B. Janowczyk, J. Rutqvist, C. F. Tsang, J. S. Y. Wang  
1279 (2014). ISRM Suggested Method for Step-Rate Injection Method for Fracture In-Situ Properties  
1280 (SIMFIP): Using a 3-Components Borehole Deformation Sensor. *Rock Mech. Rock Eng.* 47:  
1281 303–311

1282 Guglielmi Y., F. Cappa, J. Rutqvist, C.-F. Tsang, A. Thoraval (2008). Mesoscale  
1283 characterization of coupled hydromechanical behavior of a fractured-porous slope in response  
1284 to free water-surface movement. *Int. J. Rock. Mech. Min. Sci.* 42: 852–878.

1285 Guglielmi, Y., Cappa, F., Avouac, J.-P., Henry, P., and Elsworth, D. (2015). Seismicity  
1286 triggered by fluid injection induced aseismic slip. *Science*, 348(6240):1224-1226.

1287 Guglielmi, Y., F. Cappa, J. Rutqvist, C.-F. Tsang, and A. Thoraval (2006), Field and numerical  
1288 investigations of free-water surface oscillation effects on rock slope hydromechanical

Formatiert: Deutsch (Schweiz)



behaviour – consequences for rock slope stability analyses paper presented at GEOPROC 2006:  
2nd International Conference on Coupled Thermo-hydro-mechanicalchemical

Guglielmi, Y.G. and Henry, P. Nussbaum, C. Dick, P. Gout, C. Amann, F. (2015). Underground  
Research Laboratories for conducting fault activation experiments in shales. 49th US Rock  
Mechanics / Geomechanics Symposium held in San Francisco, CA, USA, ARMA 15-0489

Gupta, H. K. (1992), *Reservoir-induced Earthquakes*, 364 pp., Elsevier, Amsterdam, The  
Netherlands.

Haimson, B. C., and F. H. Cornet (2003), ISRM suggested methods for rock stress estimation-  
Part 3: hydraulic fracture (HF) and/or hydraulic testing of pre-existing fractures (HTPF), *Int. J.*  
*Rock Mech. Min. Sci.*, 40, 1011-1020.

Hampton, J. C., L. Matzar, D. Hu, and M. Gutierrez (2015), Fracture dimension investigation  
of laboratory hydraulic fracture interaction with natural discontinuity using acoustic emission,  
paper presented at 49th US Rock Mechanics/Geomechanics Symposium, American Rock  
Mechanics Association, San Francisco, 28 June-1 July.

Håring, M.O., Schanz, U., Ladner, F. & Dyer, B.C., (2008). Characterization of the Basel 1  
enhanced geothermal system, *Geothermics*, 37, 469–495.

Healy, J. H., W. W. Rubey, D. T. Griggs, and C. B. Raleigh (1968), The Denver earthquakes,  
*Science*, 161, 1301-1310.

Hickman, S. H., M. Zoback, C. A. Barton, R. Benoit, J. Svitek, Summer, and R. (2000), Stress  
and permeability heterogeneity within the Dixie Valley geothermal reservoir: recent results  
from well 82-5, paper presented at Twenty-Fifth Workshop on Geothermal Reservoir  
Engineering, Stanford University, Stanford University, Stanford, CA, Jan 24-26.

Hickman, S., M. D. Zoback, and R. Benoit (1998), Tectonic controls on fault-zone permeability  
in a geothermal reservoir at Dixie Valley, Nevada, paper 47213 presented at SPE/ISRM Eurock  
'98, Soc. of Pet. Eng., Trondheim, Norway.

Hogarth, R., H. Holl, and A. McMahon (2013), Flow testing results from Habanero EGS  
Project, paper presented at Australian Geothermal Energy Conferences, Brisbane, Australia,  
14-15 November.

Horálek, J., Z. Jechumtálová, L. Dorbath, and J. Síleny (2010), Source mechanisms of micro-  
earthquakes induced in a fluid injection experiment at the HDR site Soultz-sous-Forêts  
(Alsace) in 2003 and their temporal and spatial variations, *Geophys. J. Int.*, 181, 1547-1565  
doi: 10.1111/j.1365-246X.2010.04506.x.

1321 Houben, G. (2015), Review: Hydraulics of water wells—flow laws and influence of geometry,  
 1322 *Hydrogeology J.*, 23, 1633-1657.

1323 Hubbert, M. K. and Rubey, W. W. (1959). Role of fluid pressure in mechanics of overthrust  
 1324 faulting i. mechanics of fluid-filled porous solids and its application to overthrust faulting.  
 1325 Geological Society of America Bulletin, 70(2):115-166.

1326 Hummel, N., and T. M. Müller (2009), Microseismic signatures of non-linear pore-fluid  
 1327 pressure diffusion, *Geophys. J. Int.*, 179, 1558-1565 doi: 10.1111/j.1365-246X.2009.04373.x.

1328 Husen, S., C. Bachmann, D. Giardini (2007). Locally triggered seismicity in the central Swiss  
 1329 Alps following the large rainfall event of August 2005. *Geophysical Journal International*, 171  
 1330 (2007), pp. 1126-1134, 10.1111/j.1365-246X.2007.03561.x

1331 Huw, C., Eisner, L., Styles, P., Turner, P., (2014). Felt seismicity associated with shale gas  
 1332 hydraulic fracturing: The first documented example in Europe, *Geophysical Research Letter*,  
 1333 doi: 10.1002/2014GL062047

1334 Ishida T. (2001). Acoustic emission monitoring of hydraulic fracturing in laboratory and field.  
 1335 *Construction and Building Materials* 15 (2001). 283-295

1336 Jaeger JC. (1963). Extension Failures in Rocks subject to fluid Pressure. *Journal of Geophysical*  
 1337 *Research*, 68(21), 6066–6067.

1338 Jeanne, P., [Rutqvist, J., Rinaldi, A. P., Dobson, P. F., Walters, M., Hartline, C., & Garcia, J.](#)  
 1339 [\(2015\). Seismic and aseismic deformations and impact on reservoir permeability: The case of](#)  
 1340 [EGS stimulation at The Geysers, California, USA. \*Journal of Geophysical Research: Solid\*](#)  
 1341 [Earth, 120\(11\), 7863-7882.](#)

1342 [Jeanne, P., Rutqvist, J., Vasco, D., Garcia, J., Dobson, P. F., Walters, M., Hartline, C., Borgia,](#)  
 1343 [A. \(2014\). A 3D hydrogeological and geomechanical model of an Enhanced Geothermal](#)  
 1344 [System at The Geysers, California. \*Geothermics\*, 51, 240-252.](#)

1345 [Jeanne, P., Y. Guglielmi, and F. Cappa. 2012. Dissimilar properties within a carbonate-](#)  
 1346 [reservoir's small fault zone, and their impact on the pressurization and leakage associated with](#)  
 1347 [CO2 injection. \*Journal of Structural Geology\*. DOI:10.1016/j.jsg.2012.10.010](#)

1348 Jeffrey R, Enever J, Phillips R, Ferguson T, Davidson S, Bride J. (1993). Small-Scale Hydraulic  
 1349 Fracturing and Mineback Experiment in Coal Seams. Presented at the Proceedings of the 1993  
 1350 International Coalbed methane Symposium.

1351 Jeffrey RG, Brynes RP, Lynch PJ, Ling DJ. (1992). An Analysis of Hydraulic Fracture and  
 1352 Mineback Data for a Treatment in the German Creek Coal Seam. Society of Petroleum  
 1353 Engineers. doi:10.2118/24362-MS  
 1354 Jeffrey RG, Bungler A. (2007). A Detailed Comparison of Experimental and Numerical Data  
 1355 on Hydraulic Fracture Height Growth Through Stress Contrasts. Society of Petroleum  
 1356 Engineers. doi:10.2118/106030-MS  
 1357 Jeffrey RG, Bungler AP, Lecampion B, Zhang X, Chen ZR, van As A, et al. (2009). Measuring  
 1358 Hydraulic Fracture Growth in Naturally Fractured Rock. In 2009 SPE Annual Technical  
 1359 Conference and Exhibition (p. SPE 124919+). New Orleans, Louisiana, USA: SPE.  
 1360 Jeffrey RG, Settari A. (1995). A Comparison of Hydraulic Fracture Field Experiments,  
 1361 Including Mineback Geometry Data, with Numerical Fracture Model Simulations. Society of  
 1362 Petroleum Engineers. doi:10.2118/30508-MS  
 1363 Johnson E, Cleary MP. (1991). Implications of recent laboratory experimental results for  
 1364 hydraulic fractures. Society of Petroleum Engineers. doi:10.2118/21846-MS  
 1365 Jost M, Büßelberg T, Jost Ö, Harjes H. (1998). Source parameters of injection-induced  
 1366 microearthquakes at 9 km depth at the KTB Deep Drilling site, Germany. Bulletin of the  
 1367 Seismological Society of America, 88(3), 815–832.  
 1368 Jung R. (1989). Hydraulic in situ investigations of an artificial fracture in the Falkenberg  
 1369 Granite. Int. J. Rock Mech. Min. Sci. & Geomech. Abstr. 26: 301-308.  
 1370 Jung R. (2013). EGS — Goodbye or Back to the Future. Effective and Sustainable Hydraulic  
 1371 Fracturing, <http://dx.doi.org/10.5772/56458>  
 1372 Jupe A, Green A. S. P., Wallroth T. (1992). Induced Microseismicity and Reservoir Growth at  
 1373 the Fjällbacka Hot Dry Rocks Project, Sweden. Int. J. Rock Mech. Min. Sci. & Geomech.  
 1374 Abstr. Vol. 29. No. 4. pp. 343-354.  
 1375 Kaieda, H., Jones, R., Moriya, H., Sasaki, S. & Ushijima, K., (2005). Ogachi HDR reservoir  
 1376 evaluation by AE and geophysical methods, in Proceedings of World Geothermal Congress  
 1377 2005, Antalya, Turkey, April 24–29.  
 1378 Karvounis, D.C., Gischig, V.S., Wiemer, S., (2014). Towards a Real-Time Forecast of Induced  
 1379 Seismicity for Enhanced Geothermal Systems. Proceedings of the 2014 Shale Energy  
 1380 Engineering Conference, July 21–23, 2014, Pittsburgh, Pennsylvania, 246.

Formatiert: Englisch (USA)

1381 Keranen, K., M, Savage, H. M., Abers, G. A., & Cochran, E. S. (2013). Potentially induced  
 1382 earthquakes in Oklahoma, USA: Links between wastewater injection and the 2011 Mw 5.7  
 1383 earthquake sequence, *Geology* 41 (6), 699–702, doi:10.1130/G34045.1  
 1384 Keusen, H.R., Ganguin, J., Schuler, P., Buletti, M., 1989. Grimsel test site: Geology. Nationale  
 1385 Genossenschaft fuer die Lagerung Radioaktiver Abfaelle (NAGRA), Baden, Switzerland.  
 1386 Technical Report NTB 87-14E, 166 pp.  
 1387 Király, E., Zecher, J.D., Gischig, V.S, Karvounis, D., Doetsch, J., Wiemer, S., (2015). Modeling  
 1388 Induced Seismicity and Validating Models in Deep Geothermal Energy Projects. In  
 1389 preparation.  
 1390 Kohl, T., K. F. Evans, R. J. Hopkirk, R. Jung, and L. Rybach (1997), Observation and  
 1391 simulation of non-Darcian flow transients in fractured rock, *Wat. Resour. Res.*, 33(3), 407-  
 1392 418.  
 1393 Krietsch, H., V. Gischig, R. Jalali, F. Amann, K. F. Evans, J. Doetsch, and B. Valley (2017),  
 1394 Stress measurements in crystalline rock: Comparison of overcoring, hydraulic fracturing and  
 1395 induced seismicity results, in *ARMA 51st US Rock Mechanics / Geomechanics Symposium*,  
 1396 edited, San Francisco, California, USA.  
 1397 Lee, H. S., and T. F. Cho (2002), Hydraulic Characteristics of Rough Fractures in Linear Flow  
 1398 under Normal and Shear Load, *Rock Mech. Rock Eng.*, 35, 299-318 DOI 10.1007/s00603-002-  
 1399 0028-y.  
 1400 Lee, H.S., Cho, T.F. (2002). Hydraulic characteristics of rough fractures in linear flow under  
 1401 normal and shear load, *Rock Mech. Rock Eng.*, 35(4), 299–318.  
 1402 Louis, C., J.-L., Dessene, B. Feuga (1977). Interaction between water flow phenomena and the  
 1403 mechanical behavior of soil or rock masses. Gudehns, G., ed., *Finite elements in geomechanics*:  
 1404 New York, John Wiley S Sons, 572 p.  
 1405 Majer, E., J. Nelson, A. Robertson-Tait, J. Savy, and I. Wong (2012). Protocol for addressing  
 1406 induced seismicity associated with enhanced geothermal systems, U.S. Department of Energy,  
 1407 Energy Efficiency and Renewable Energy.  
 1408 Manning, C. and Ingebritsen, S. (1999). Permeability of the continental crust: Implications of  
 1409 geothermal data and metamorphic systems. *Reviews of Geophysics*, 37(1):127/150.  
 1410 Marone, C., and C. H. Scholz (1988), The depth of seismic faulting and the upper transition  
 1411 from stable to unstable slip regimes, *Geophys. Res. Lett.*, 15(6), 621-624 DOI:  
 1412 10.1029/GL015i006p00621.

1413 [Martínez-Garzón, P., Kwiatak, G., Bohnhoff, M., & Dresen, G. \(2017\). Volumetric components](#)  
 1414 [in the earthquake source related to fluid injection and stress state. \*Geophysical Research Letters\*,](#)  
 1415 [44\(2\), 800-809.](#)

1416 [Martínez-Garzón, P., Bohnhoff, M., Kwiatak, G., & Dresen, G. \(2013\). Stress tensor changes](#)  
 1417 [related to fluid injection at The Geysers geothermal field, California. \*Geophysical Research\*](#)  
 1418 [Letters, 40\(11\), 2596-2601.](#)

1419 Martin C. D., C. C. Davison, E. T. Kozak (1990). Characterizing normal stiffness and hydraulic  
 1420 conductivity of a major shear zone in granite. Rock joints, eds. Barton & Stephansson, Balkema,  
 1421 Rotterdam, Netherlands.

1422 Maury, V., 1994. Rock failure mechanisms identification: A key for wellbore stability and  
 1423 reservoir behaviour problem, in Eurock 94, edited by Delft, Netherlands, 29-31 August, 175-  
 1424 182, Balkema.

1425 Maxwell, S. (2014), Microseismic Imaging of Hydraulic Fracturing: Improved Engineering of  
 1426 Unconventional Shale Reservoirs, 197 pp., Society of Exploration Geophysicists.

1427 McClure, M. W. (2015), Generation of large postinjection-induced seismic events by backflow  
 1428 from dead-end faults and fractures, *Geophysical Research Letters*, 42(6647–6654).

1429 McClure M.W., R. N. Horne (2011). Investigation of injection-induced seismicity using a  
 1430 coupled fluid flow and rate/state friction model. *Geophysics* 76, 6.

1431 McClure M.W., R. N. Horne (2014). An investigation of stimulation mechanisms in Enhanced  
 1432 Geothermal Systems *International Journal of Rock Mechanics & Mining Sciences* 72: 242–260

1433 McClure, M. W. (2012). Modeling and characterization of hydraulic stimulation and induced  
 1434 seismicity in geothermal and shale gas reservoirs. PhD thesis, Stanford University.

1435 McGarr, A. (1976). Seismic moments and volume changes, *Journal of Geophysical Research*,  
 1436 81(8), 1487-1494.

1437 Mena, B., Wiemer, S., Bachmann, C., (2013). Building robust model to forecast the induced  
 1438 seismicity related to geothermal reservoir enhancements, *Bull. seism. Soc. Am.*, 103(1), 383–  
 1439 393.

1440 Meng, C. (2011), Hydraulic fracture propagation in pre-fractured rocks, paper presented at SPE  
 1441 Hydraulic Fracturing Technology Conference and Exhibition, SPE, The Woodlands, Texas,  
 1442 24-26 Jan.

Formatiert: Englisch (USA)

1443 Mignan, A., Landtwing, D., Kästli, P., Mena, B., Wiemer, S. (2015). Induced seismicity risk  
1444 analysis of the 2006 Basel, Switzerland, Enhanced Geothermal System project: Influence of  
1445 uncertainties on risk mitigation, *Geothermics*, 53 (2015) 133–146.

1446 Murdoch LC, Schweisinger T, Svenson E, Germanovich L. (2004). Measuring and analyzing  
1447 transient changes in fracture aperture during well tests: preliminary results. In: *Dynamics of*  
1448 *fluids in fractured rock (Witherspoon Conference)*. LBL Report 54275, February 10–14, 2004.  
1449 p. 129–32.

1450 Murphy H., C. Huang, Z. Dash, G. Zyvoloski, A. White (2004). Semi-analytical solutions for  
1451 fluid flow in rock joints with pressure-dependent openings. *Water Resources Research* 40,  
1452 W12506

1453 Nicholson, C., and R. L. Wesson (1990), Earthquake Hazard Associated with Deep Well  
1454 Injection-A Report to the U.S. Environmental Protection Agency, 1951, US Geological Survey  
1455 Bulletin.

1456 Nicol, D. A. C., and B. A. Robinson (1990), Modelling the heat extraction from the  
1457 Rosemanowes HDR reservoir, *Geothermics*, 19, 247-257.

1458 Niitsuma H., M. Fehler, R. Jones, S. Wilson, J. Albright, A. Green, R. Baria, K. Hayashi, H.  
1459 Kaieda, K. Tezuka, A. Jupe, T. Wallroth, F. Cornet, H. Asanuma, H. Moriya, K. Nagano, W.S.  
1460 Phillips, J. Rutledge, L. House, A. Beauce, D. Alde, R. Aster (1999). Current status of seismic  
1461 and borehole measurements for HDR/HWR development. *Geothermics*, 28, 4-5: 475-490.

1462 Olsson R., N. Barton (2001). An improved model for hydromechanical coupling during  
1463 shearing of rock joints. *International Journal of Rock Mechanics and Mining Sciences*, 38, 3:  
1464 317–329.

1465 Parker R. (1999). The Rosemanowes HDR project 1983-1991. *Geothermics*, 28, 603-615.

1466 Parker, R. H. (1989a), Hot Dry Rock Geothermal Energy: Phase 2B Final Report of the  
1467 Camborne School of Mines Project, 1391 pp., Pergamon Press, Oxford.

1468 Pearson, C. (1981), The relationship between microseismicity and high pore pressures during  
1469 hydraulic stimulation experiments in low porosity granitic rock, *J. Geophys. Res.*, 86, 7855-  
1470 7864.

1471 Pettitt W, Pierce M, Damjanac B, Hazzard J, Lorig L, Fairhurst C, et al. (2011). Fracture  
1472 network engineering for hydraulic fracturing. *The Leading Edge*, 30(8), 844–853.  
1473 doi:10.1190/1.3626490

1474 Petty, S., Nordin, Y., Glassely, W., Cladouhos, T. (2013). Improving geothermal project  
 1475 economics with multi-zone stimulation: results from the Newberry volcano EGS  
 1476 demonstration. Proc. 38th Works. Geoth. Rese. Eng., Stanford University, SGP-TR-198.  
 1477 Phillips, S., L. S. House, and M. C. Fehler (1997), Detailed joint structure in a geothermal  
 1478 reservoir from studies of induced microseismic clusters, *J. Geophys. Res.*, 102(B6), 11,745-  
 1479 711,763.  
 1480 Pine, R.J., Baria, R., Pearson, R.A., Kwakwa, K., McCartney, R (1987). A Technical Summary  
 1481 of Phase 2B of the Camborne School of Mines HDR Project, 1983-1986. *Geothermics*, 16, 4:  
 1482 341-353.  
 1483 Potter, R., Robinson, E., and Smith, M. (1974). Method of extracting heat from dry geothermal  
 1484 reservoirs. US Patent 3,786,858.  
 1485 Power, W. L., and T. E. Tullis (1991), Euclidean and fractal models for the description of  
 1486 surface roughness, *J. Geophys. Res.*, 96(B1), 415-424.  
 1487 Preisig, G., E. Eberhardt, V. Gischig, V. Roche, M. Van der Baan, B. Valley, P. Kaiser, and D.  
 1488 Du (2015), Development of connected rock mass permeability by hydraulic fractures growth  
 1489 accompanying fluid injection, *Geofluids* 15, 321–337. Rahman, M.K., Hossain, M.M.,  
 1490 Rahman, S.S. (2002). A shear-dilation-based model for evaluation of hydraulically stimulated  
 1491 naturally fractured reservoirs. *International Journal for Numerical and Analytical Methods in*  
 1492 *Geomechanics*, 26, 5: 469-497.  
 1493 Pruess, K., (2006). Enhanced geothermal systems (EGS) using CO<sub>2</sub> as working fluid – a novel  
 1494 approach for generating renewable energy with simultaneous sequestration of carbon.  
 1495 *Geothermics* 35 (4), 351–367.  
 1496 Pruess, K., (2007). Role of fluid pressure in the production behavior of enhanced geothermal  
 1497 systems with CO<sub>2</sub> as working fluid. *GRC Trans.* 31, 307–311.  
 1498 Raleigh, C., Healy, J., and Bredehoeft, J. (1976). An experiment in earthquake control at  
 1499 Rangely, Colorado. *work (Fig. 1b)*, 108(52):30.  
 1500 Randolph, J.B., and M.O. Saar (2011a), Combining geothermal energy capture with geologic  
 1501 carbon dioxide sequestration, *Geophysical Research Letters*, DOI: 10.1029/2011GL047265,  
 1502 38, L10401.

1503 Randolph, J.B. and M.O. Saar (2011b). Coupling carbon dioxide sequestration with geothermal  
 1504 energy capture in naturally permeable, porous geologic formations: Implications for CO<sub>2</sub>  
 1505 sequestration, *Energy Procedia*, DOI: 10.1016/j.egypro.2011.02.108, 4:2206-2213.

1506 Rutledge, J. T., Phillips, W. S., & Mayerhofer, M. J.: Faulting Induced by Forced Fluid  
 1507 Injection and Fluid Flow Forced by Faulting: An Interpretation of Hydraulic-Fracture  
 1508 Microseismicity, Carthage Cotton Valley Gas Field, Texas, *Bulletin of the Seismological*  
 1509 *Society of America*, 94, (2004),1817.

1510 Rutqvist J. (1995): Determination of hydraulic normal stiffness of fractures in hard rock from  
 1511 well testing. *Int. J. Rock Mech. Min. Sci.* 1, 32: 513–23.

1512 Rutqvist J., O. Stephansson (2003). The role of hydromechanical coupling in fractured rock  
 1513 engineering. *Hydrogeology Journal*, 11, 1:7–40.

1514 Rutqvist, J. (2011). Status of the tough-ac simulator and recent applications related to coupled  
 1515 fluid flow and crustal deformations. *Computers & Geosciences*, 37(6):739-750.

1516 Rutqvist, J., and C. M. Oldenburg (2008), Analysis of injection-induced micro-earthquakes in  
 1517 a geothermal steam reservoir, Geysers Geothermal Field, California, *Proceedings of the 42th*  
 1518 *U. S. Rock Mechanics Symposium*, June 29–July 2, 2008, San Francisco, California, USA, 151.

1519 Rutqvist, J., and O. Stephansson (1996), A cyclic hydraulic jacking test to determine the in-situ  
 1520 stress normal to a fracture, *Int. J. Rock Mech. Min. Sci. & Geomech. Abstr.*, 33(7), 695-711.

1521 Saar, M.O., and M. Manga (2003). Seismicity induced by seasonal groundwater recharge at Mt.  
 1522 Hood, Oregon, *Earth and Planetary Science Letters*, DOI: 10.1016/S0012-821X(03)00418-7,  
 1523 214:605-618.

1524 Saar, M.O., and M. Manga (2004). Depth dependence of permeability in the Oregon Cascades  
 1525 inferred from hydrogeologic, thermal, seismic, and magmatic modeling constraints, *Journal of*  
 1526 *Geophysical Research*, DOI: 10.1029/2003JB002855, 109, Nr. B4, B04204.

1527 Saar, M.O. (2011). Review: Geothermal heat as a tracer of large-scale groundwater flow and  
 1528 as a means to determine permeability fields, *Hydrogeology Journal*, DOI: 10.1007/s10040-010-  
 1529 0657-2, 19:31-52, 2011.

1530 Saar, M.O. (~~to be published~~ 2017). Novel Geothermal Technologies, in *Potentials, costs and*  
 1531 *environmental assessment of electricity generation technologies*, edited by C. Bauer and S.  
 1532 Hirschberg, Swiss Federal Office of Energy, Swiss Competences Center for Energy Research  
 1533 "Supply of Electricity", Swiss Competence Center for Energy Research "Biomass for Swiss  
 1534 Energy Future".

Formatiert: Englisch (Großbritannien)



1535 [Samuelson, J., Elsworth, D., & Marone, C. \(2009\). Shear-induced dilatancy of fluid-saturated](#)  
 1536 [faults: Experiment and theory. Journal of Geophysical Research: Solid Earth, 114\(B12\).](#)  
 1537 Schanz U, Dyer B, Ladner F, Haering MO. (2007). Microseismic aspects of the Basel 1  
 1538 geothermal reservoir. In 5th Swiss Geoscience Meeting. Geneva.  
 1539 Schmittbuhl, J., F. Schmitt, and C. H. Scholz (1995), Scaling invariance of crack surfaces, *J.*  
 1540 *Geophys. Res.*, 100(B4), 5953-5973.  
 1541 Schoenball, M., Baujard, C., Kohl, T., Dorbath, L. (2012). The role of triggering by static stress  
 1542 transfer during geothermal reservoir stimulation, *J. geophys. Res.*, 117, B09307.  
 1543 Scholz, C. H. (2015), On the stress dependence of the earthquake b value, *Geophys. Res.Lett.*,  
 1544 42, 1399-1402 doi:10.1002/2014GL062863.  
 1545 Scholz, C.H., 1990. The mechanics of Earthquakes and Faulting. Cambridge University Press,  
 1546 Cambridge, UK, p. 39.  
 1547 Schorlemmer, D., S. Wiemer, Wyss, M., (2005). Variations in earthquake size distribution  
 1548 across different stress regimes, *Nature*, 437, 539–542.  
 1549 Schrauf T. W., Evans D. D. (1986). Laboratory Studies of Gas Flow Through a Single Natural  
 1550 Fracture WATER RESOURCES RESEARCH, VOL. 22, NO. 7, 1038-1050  
 1551 Schweisinger T., E.J. Swenson, L.C. Murdoch (2009): Introduction to hydromechanical well  
 1552 tests in fractured rock aquifers. *Groundwater* 47, 1:69–79  
 1553 Schweisinger, T., L.C. Murdoch, and C.O. Huey Jr. (2007). Design of a removable borehole  
 1554 extensometer. *Geotechnical Testing Journal* 30, no. 3: 202–211.  
 1555 Scotti O., Cornet F.H. (1994). In situ evidence for fluid induced aseismic slip events along fault  
 1556 zones. *Int J Rock Mech Min* 1:347-358.  
 1557 Shamir, G., and M. D. Zoback (1992), Stress orientation profile to 3.5 km depth near the San  
 1558 Andreas fault at Cajon Pass, California, *J. Geophys. Res.*, 97, 5059-5080.  
 1559 Sileny, J., D. P. Hill, and F. H. Cornet (2009), Non-double-couple mechanisms of  
 1560 microearthquakes induced by hydraulic fracturing, *J. Geophys. Res.*, 114, B08307  
 1561 doi:10.1029/2008JB005987.  
 1562 Song I, Suh M, Won K, Haimson B. (2001). A laboratory study of hydraulic fracturing  
 1563 breakdown pressure in tablerock sandstone. *Geosciences Journal*, 5(3), 263–271.  
 1564 doi:10.1007/bf02910309

1565 Spada, M., Tormann, T., Goebel, T., Wiemer, S. (2013). Generic dependence of the frequency-  
 1566 size distribution of earthquakes on depth and its relation to the strength profile of the crust,  
 1567 Geophys. Res. Lett., 40(4), 709–714.

1568 Stein, R. S. (1999). The role of stress transfer in earthquake occurrence. *Nature*, 402(6762):  
 1569 605-609.

1570 Tenma N., Yamaguchi T., Zyvoloski G. (2008). The Hijiori Hot Dry Rock test site, Japan  
 1571 evaluation and optimization of heat extraction from a two-layered reservoir. *Geothermics* 2008;  
 1572 37:19–52.

1573 Terakawa, T., Miller, S.A., Deichmann, N. (2012). High fluid pressure and triggered  
 1574 earthquakes in the enhanced geothermal system in Basel, Switzerland, *J. Geophys. Res.*, 117,  
 1575 B07305.

1576 Tester, J. W., Anderson, B. J., Batchelor, A., Blackwell, D., DiPippo, R., Drake, E., Garnish, J.,  
 1577 Livesay, B., Moore, M., Nichols, K., et al. (2006). The future of geothermal energy. Impact of  
 1578 Enhanced Geothermal Systems (EGS) on the United States in the 21st Century, Massachusetts  
 1579 Institute of Technology, Cambridge, MA, page 372.

1580 Tezuka, K., and H. Niitsuma (2000), Stress estimated using microseismic clusters and its  
 1581 relationship to the fracture system of the Hijiori Hot Dry Rock reservoir, *Engineering Geology*,  
 1582 56, 47-62.

1583 Tormann, T., B Enescu, J. Woessner and S. Wiemer (2015). Randomness of megathrust  
 1584 earthquakes implied by rapid stress recovery after the Japan earthquake, *Nature Geoscience* 8  
 1585 (2), 152-158.

1586 Tormann, T., S. Wiemer, A. Mignan (2014). Systematic survey of high-resolution b value  
 1587 imaging along Californian faults: Inference on asperities, *J. Geophys. Res. Solid Earth*, 119(3),  
 1588 2029–2054.

1589 Valley, B., and K. F. Evans (2009), Stress orientation to 5 km depth in the basement below  
 1590 Basel (Switzerland) from borehole failure analysis, *Swiss J. Earth Sci.*, 102, 467-480 doi:  
 1591 10.1007/s00015-009-1335-z.

1592 Valley, B., and K. F. Evans (2010), Stress Heterogeneity in the Granite of the Soultz EGS  
 1593 Reservoir Inferred from Analysis of Wellbore Failure, paper presented at World Geothermal  
 1594 Congress, International Geothermal Association, Bali, 25-29 April 2010

1595 van As A, Jeffrey R. (2002). Hydraulic fracture growth in naturally fractured rock: mine  
 1596 through mapping and analyses. Presented at the NARMS-TAC conference, Toronto, Canada.

1597 van As A, Jeffrey RG. (2000). Caving Induced by Hydraulic Fracturing at Northparkes Mines.  
 1598 Presented at the 4th North American Rock Mechanics Symposium, American Rock Mechanics  
 1599 Association. <https://www.onepetro.org/conference-paper/ARMA-2000-0353>. Accessed 26  
 1600 September 2015

1601 van As, A., Jeffrey R., Chacón E. and Barrera, V. (2004). Preconditioning by hydraulic  
 1602 fracturing for bloc caving in a moderately stressed naturally fractured orebody. Proceeding of  
 1603 the Massmin 2004 conference, Santiago Chile, 22-25 August 2004.

1604 van der Baan M, Eaton D, Dusseault M. (2013). Microseismic Monitoring Developments in  
 1605 Hydraulic Fracture Stimulation. In R Jeffrey (Ed.), Effective and Sustainable Hydraulic  
 1606 Fracturing. InTech. [http://www.intechopen.com/books/effective-and-sustainable-hydraulic-](http://www.intechopen.com/books/effective-and-sustainable-hydraulic-fracturing/microseismic-monitoring-developments-in-hydraulic-fracture-stimulation)  
 1607 fracturing/microseismic-monitoring-developments-in-hydraulic-fracture-stimulation.  
 1608 Accessed 25 September 2015

1609 Vermeylen J, Zoback MD. (2011). Hydraulic Fracturing, Microseismic Magnitudes, and Stress  
 1610 Evolution in the Barnett Shale, Texas, USA. Society of Petroleum Engineers.  
 1611 doi:10.2118/140507-MS

1612 Vogler D., Amann F., Bayer P., Elsworth D. (2015). Permeability Evolution in Natural  
 1613 Fractures Subject to Cyclic Loading and Gouge Formation. RMRE, 49(9).

1614 Warpinski N. (2009). Microseismic Monitoring: Inside and Out. Journal of Petroleum  
 1615 Technology, 61(11), 80–85. doi:10.2118/118537-JPT

1616 Warpinski N. (2013). Understanding Hydraulic Fracture Growth, Effectiveness, and Safety  
 1617 Through Microseismic Monitoring. In R Jeffrey (Ed.), Effective and Sustainable Hydraulic  
 1618 Fracturing. InTech. [http://www.intechopen.com/books/effective-and-sustainable-hydraulic-](http://www.intechopen.com/books/effective-and-sustainable-hydraulic-fracturing/understanding-hydraulic-fracture-growth-effectiveness-and-safety-through-microseismic-monitoring)  
 1619 [fracturing/understanding-hydraulic-fracture-growth-effectiveness-and-safety-through-](http://www.intechopen.com/books/effective-and-sustainable-hydraulic-fracturing/understanding-hydraulic-fracture-growth-effectiveness-and-safety-through-microseismic-monitoring)  
 1620 [microseismic-monitoring.](http://www.intechopen.com/books/effective-and-sustainable-hydraulic-fracturing/understanding-hydraulic-fracture-growth-effectiveness-and-safety-through-microseismic-monitoring) Accessed 26 September 2015

1621 Warpinski N., L. W. Teufel (1987): Influence of geologic discontinuities on hydraulic fracture  
 1622 propagation. J. Petrol. Technol. 39: 209–20

1623 Warpinski NR, Clark JA, Schmidt RA, Huddle CW. (1982). Laboratory Investigation on the -  
 1624 Effect of In-Situ Stresses on Hydraulic Fracture Containment. Society of Petroleum Engineers  
 1625 Journal, 22(03), 333–340. doi:10.2118/9834-PA

1626 Warpinski NR, Du J. (2010). Source-Mechanism Studies on Microseismicity Induced by  
 1627 Hydraulic Fracturing. Society of Petroleum Engineers. doi:10.2118/135254-MS

Formatiert: Deutsch (Schweiz)

1628 Warpinski NR. (1985). Measurement of Width and Pressure in a Propagating Hydraulic  
1629 Fracture. Society of Petroleum Engineers Journal, 25(01), 46–54. doi:10.2118/11648-PA

1630 Warren W. E., Schmith C. W. (1985). In Situ Stress Estimates From Hydraulic Fracturing and  
1631 Direct Observation of Crack Orientation. Journal of Geophysical Research, Vol. 9, NO. B8,  
1632 829-68

1633 Wehrens, P. (2015). Structural evolution in the Aar Massif (Haslital transect): Implications for  
1634 the mid-crustal deformation. PhD thesis, University Bern.

1635 Wolhart, S. L., T. A. Harting, J. E. Dahlem, T. Young, M. J. Mayerhofer, and E. P. Lolon  
1636 (2006), Hydraulic fracture diagnostics used to optimize development in the Jonah field, paper  
1637 presented at SPE Annual Technical Conference and Exhibition. Society of Petroleum  
1638 Engineers.

1639 Yeo I. W., M. H. De Freitas, and R. W. Zimmerman (1998). Effect of shear displacement on  
1640 the aperture and permeability of a rock fracture. International Journal of Rock Mechanics and  
1641 Mining Sciences, 35, 8:1051–1070

1642 Yoon, J.-S., Zang, A., Stephansson, O., 2014. Numerical investigation on optimized stimulation  
1643 of intact and naturally fractured deep geothermal reservoirs using hydro-mechanical coupled  
1644 discrete particles joints model. Geothermics, 52.

1645 Zang A, Yoon J.S., Stephansson O, Heidbach O. (2013). Fatigue hydraulic fracturing by cyclic  
1646 reservoir treatment enhances permeability and reduces induced seismicity. Geophysical Journal  
1647 International, 195(2), 1282–1287. doi:10.1093/gji/ggt301

1648 Zang A., Stephansson O. (2013). Stress Field of the Earth's Crust. Springer Dordrecht  
1649 Heidelberg London New York, DOI 10.1007/978-1-4020-8444-7.

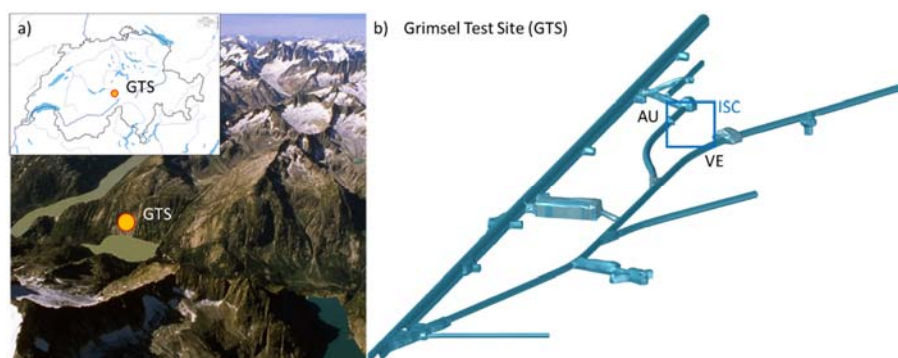
1650 Ziegler M, Valley B, Evans K. (2015). Characterisation of Natural Fractures and Fracture Zones  
1651 of the Basel EGS Reservoir Inferred from Geophysical Logging of the Basel-1 Well. Presented  
1652 at the Proceedings World Geothermal Congress 2015.

1653 Zoback, M. D. and Harjes, H.-P. (1997). Injection-induced earthquakes and crustal stress at 9  
1654 km depth at the KTB deep drilling site, Germany. Journal of Geophysical Research: Solid Earth,  
1655 102(B8):18477-18491.

1656 Zoback, M. D., Kohli, A., Das, I., McClure, M. W., et al. (2012). The importance of slow slip  
1657 on faults during hydraulic fracturing stimulation of shale gas reservoirs. In SPE Americas  
1658 Unconventional Resources Conference. Society of Petroleum Engineers.

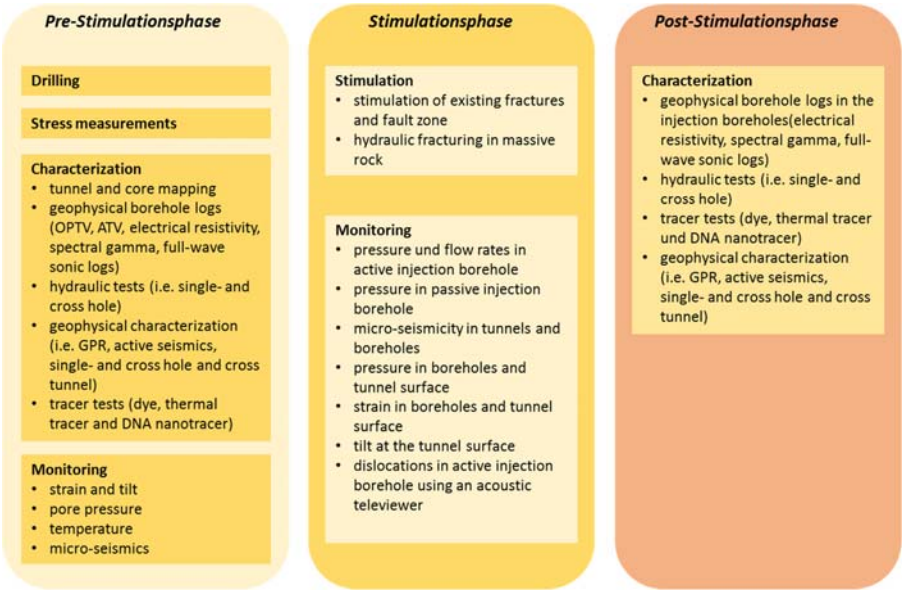
1659 Zoback, M.D., Rummel, F., Jung R., Raleigh C.B. (1977). Laboratory Hydraulic Fracturing  
1660 Experiments in Intact and Pre-fractured Rock Int. J. Rock Mech. Min. Sci. & Geomech. Abstr.  
1661 Vol. 14, pp. 49-58.

1662  
1663  
1664  
1665  
1666  
1667  
1668  
1669  
1670  
1671  
1672  
1673  
1674  
1675  
1676



1677  
1678 *Figure 1. a) Grimsel Test Site (GTS) is located in the Swiss Alps in the central part of Switzerland. b)*  
1679 *The in-situ stimulation and circulation experiment (ISC experiment) is implemented in the southern*  
1680 *part of the GTS in a low fracture density granitic rock*

1681



1682

1683 *Figure 2. The three test phases of the ISC experiments with listings of the main activities*  
1684 *during each phase.*

1685

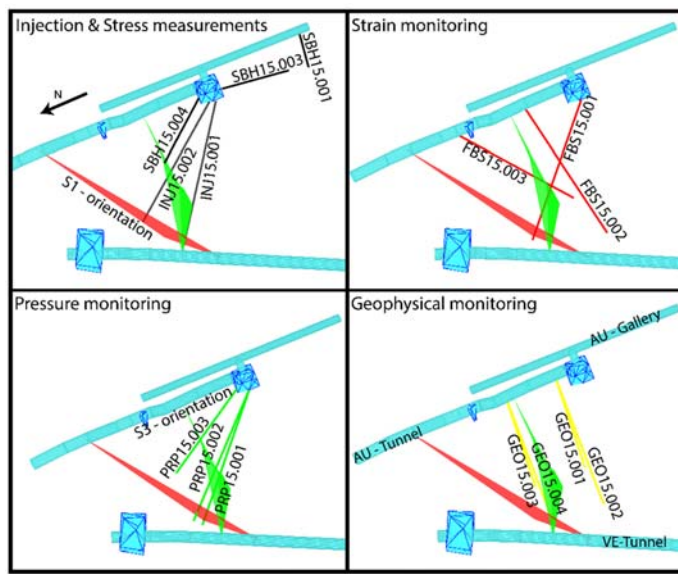
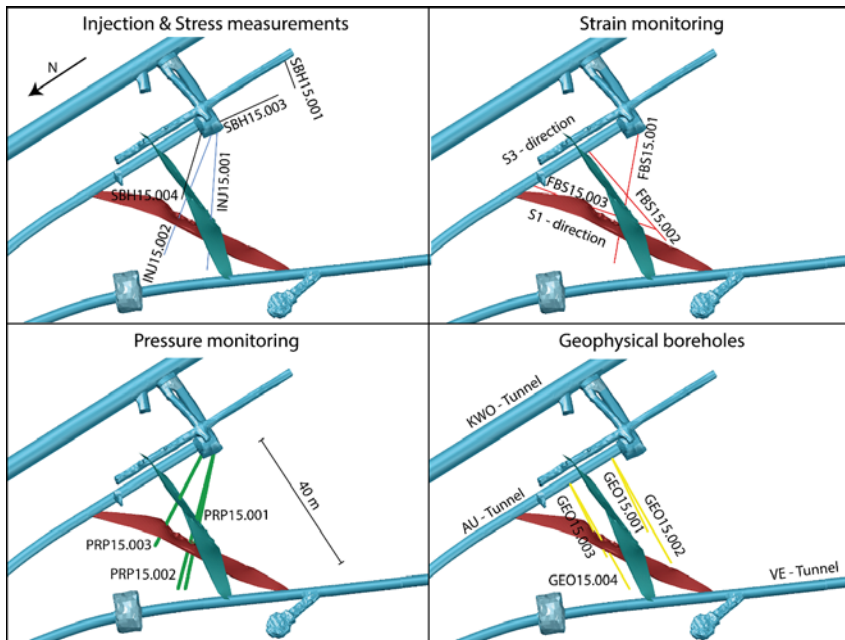


Figure 3: The 15 boreholes drilled for the ISC experiment (view steeply inclined towards SE).

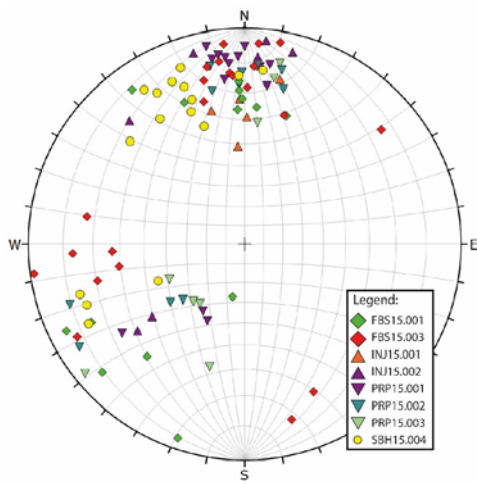


Figure 4. Brittle fractures between meta basic dykes plotted into the lower hemisphere of a stereonet plot. The data set is subdivided into the borehole where they were observed.



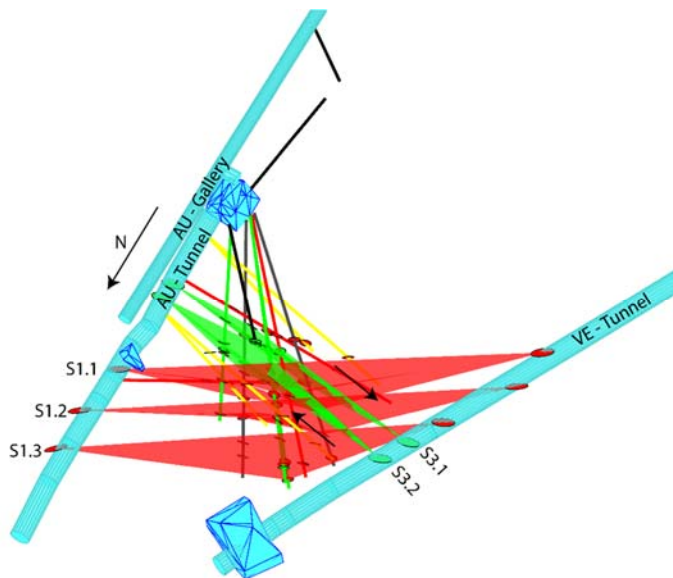
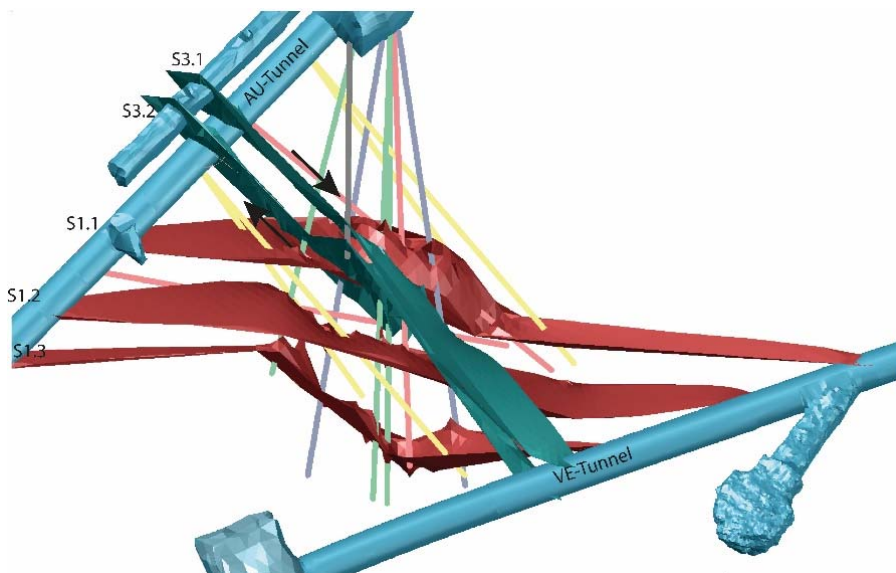
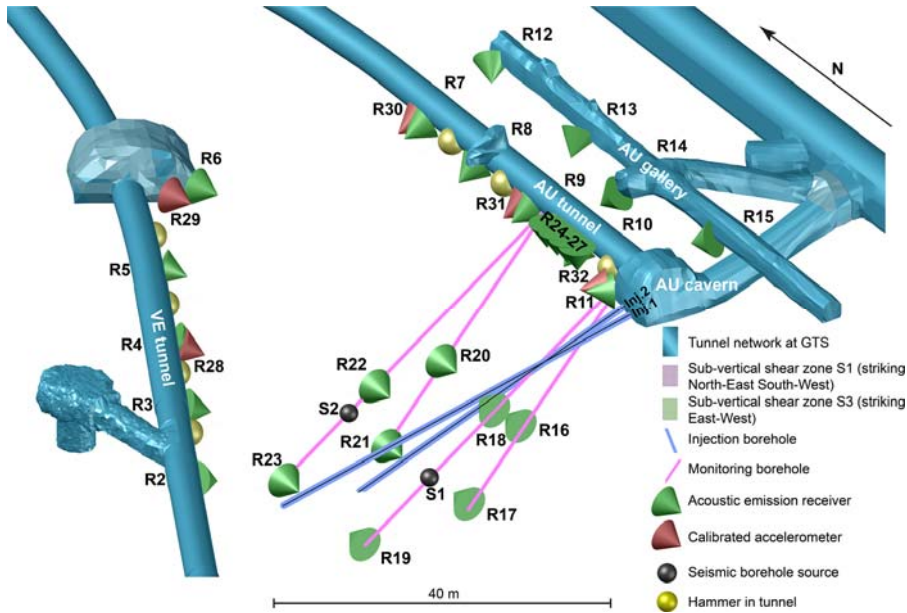


Figure 5:

Figure 4: 3D-Model showing the boreholes drilled towards the rock volume for the in-situ stimulation experiment, S1 (red) and S3 (bluegreen) oriented shear zones as well as the dextral shear sense at the S3 shear zones indicated by the black arrows.



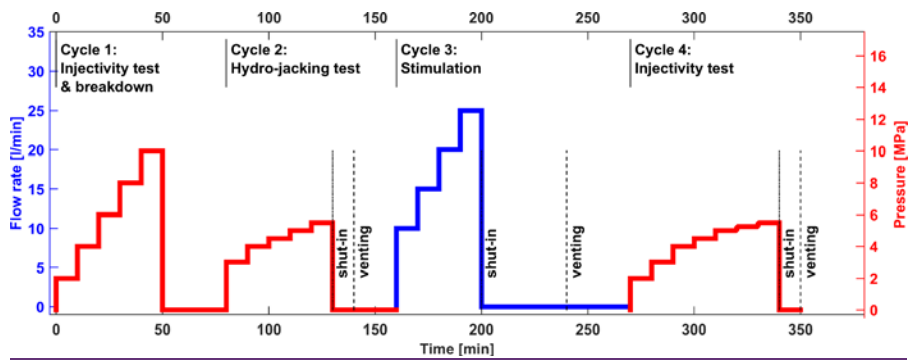
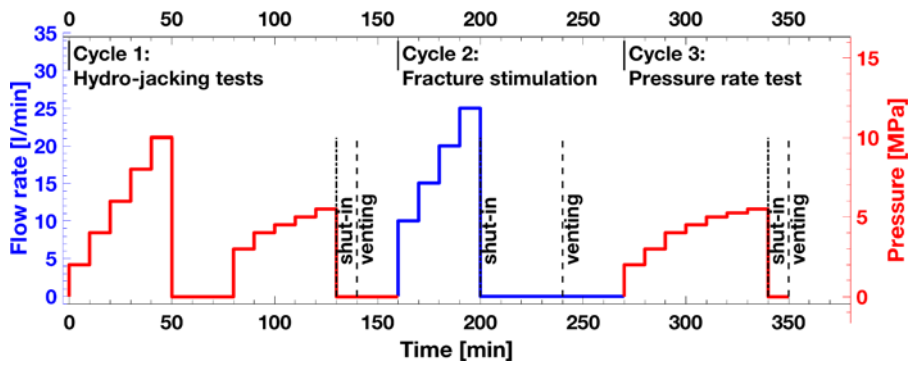
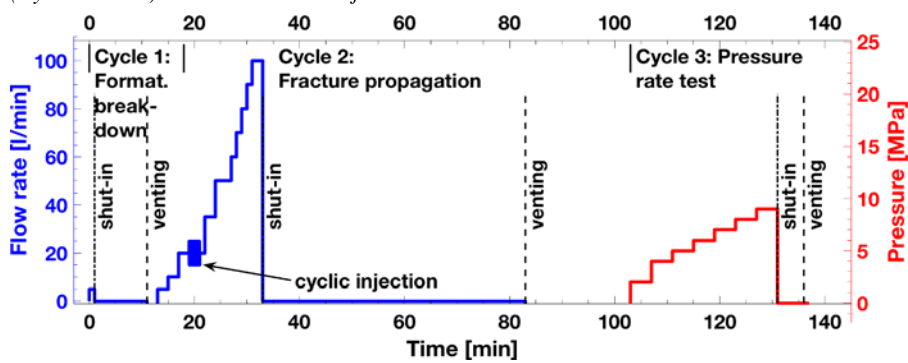


Figure 7: Planned injection protocol for hydroshearing experiments. Red curves denote pressure controlled injections. (Cycle 1), blue curves flow rate controlled injections (Cycle 2 and 3). The total volume injected is  $1 \text{ m}^3$ .



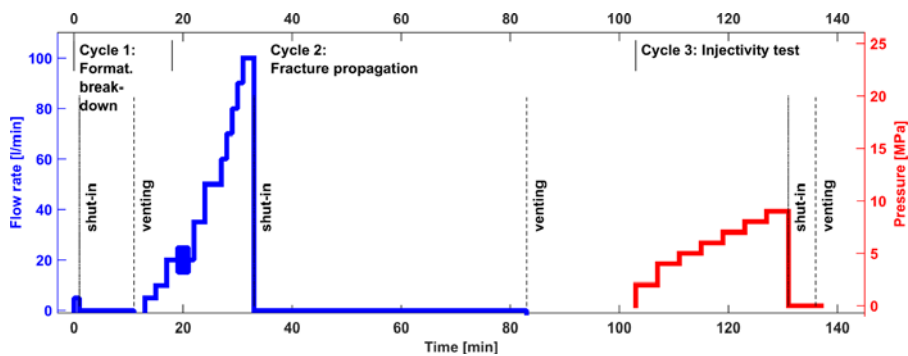


Figure 8: Planned injection protocol for hydrofracturing experiments. The blue solid curve denotes flow rate controlled and the red solid curve pressure controlled injection. The red dashed line respective the blue dashed line are the anticipated pressure respective flow rate response.